

# Catchment transit time ~~sensitivity to the type of~~ variability with different SAS function parameterizations for the unsaturated zone and groundwater

Hatice Türk<sup>1</sup>, Christine Stumpff<sup>1</sup>, Markus Hrachowitz<sup>2</sup>, Peter Strauss<sup>3</sup>, Günter Blöschl<sup>4</sup>, and Michael Stockinger<sup>1</sup>

<sup>1</sup>BOKU University, Institute of Soil Physics and Rural Water Management, Department of Landscape, Water and Infrastructure, Muthgasse 18, 1190 Vienna, Austria

<sup>2</sup>Department of Water Management, Faculty of Civil Engineering and Geosciences, Delft University of Technology, Stevinweg 1, 2628 CN Delft, the Netherlands

<sup>3</sup>Institute for Land and Water Management Research, Federal Agency for Water Management, Petzenkirchen, Austria

<sup>4</sup>Vienna University of Technology, Institute of Hydraulic Engineering and Water Resources Management, Karlsplatz 13, 1040 Vienna, Austria

**Correspondence:** Hatice Türk (hatice.tuerk@boku.ac.at)

**Abstract.** Preferential flow paths in hydrological systems (e.g., macropores or subsurface pipe networks) facilitate ~~rapid water and solute transport, leading to fast streamflow responses and markedly~~ the rapid transmission of precipitation and solutes to streams, resulting in streamflow responses characterized by the release of young water (i.e., recent precipitation) from the catchment and correspondingly short transit times ~~. While such preferential flow processes are well known in~~ (on the order of  
5 days). While preferential flow paths are documented in both the unsaturated zone and groundwater, it remains uncertain whether catchment-scale isotope-based transport models can ~~accurately represent these fast groundwater flow processes~~ adequately represent preferential flow using tracer measurements in streamflow. In this study, we ~~tested the hypothesis that preferential discharge of young groundwater is significant and can be captured by selecting specific~~ hypothesized that the preferential release of young water from both the unsaturated zone and groundwater contributes measurably to the streamflow tracer signal.  
10 This effect can be represented through StorAge Selection (SAS) functions, ~~i.e., functions that specify if~~ which specify how young or old water leaves a storage, ~~at the catchment scale~~. We systematically compared multiple ~~SAS parameterisations~~ parameterizations of the SAS functions for the unsaturated zone and groundwater ~~using a catchment-scale transport model and within a single catchment-scale transport model using~~ long-term measurements of hydrogen isotopes in water ( $\delta^2\text{H}$ ) ~~data~~ from two headwater catchments (the Hydrological Open Air Laboratory ~~, HOAL, catchment (HOAL)~~ in Austria and the  
15 Wüstebach catchment in Germany). The results indicated that  $\delta^2\text{H}$  ~~ratios in streamflow had sufficient information content to identify preferential flow~~ measurements in streamflow exhibited sufficient variability to confirm the preferential release of young water through preferential flow paths in the unsaturated zone. ~~However,~~ This interpretation was supported by Spearman rank correlations ( $r$ ) between simulated and observed  $\delta^2\text{H}$  ratios in streamflow were insufficient to constrain or confirm preferential flow in groundwater signals in streamflow, where  $r$  values ranged from 0.58 to  $-0.18$  for the HOAL catchment  
20 and from 0.58 to 0.28 for the Wüstebach catchment, corresponding to SAS shape parameters that reflected a transition from

a strong young-water preference to an old-water preference. However, contrary to the unsaturated zone, the variability of  $\delta^{2}\text{H}$  in streamflow was not sufficient to confirm the preferential release of young water from groundwater storage, as any seasonal variation of  $\delta^{2}\text{H}$  in pore water was largely dampened by the catchments' substantial passive groundwater storage volumes. This was further confirmed as the observed attenuated  $\delta^{2}\text{H}$ , with  $r$  values ranging between 0.54 and 0.60 in the HOAL, and ranging between 0.71 and 0.76 in the Wüstebach catchment. This interpretation was further supported by the fact that the observed attenuated  $\delta^{2}\text{H}$  signal in streamflow could only be simulated-reproduced when the volume ratio between active and passive groundwater storage was  $\ll$  less than 1 %. This damping effect affected the %, highlighting the dependence of SAS-based age selection on storage configuration. The damping effect, in combination with the groundwater SAS function parameterization, influenced the estimation of the longer tails ( $100 < T < 1000$  days) of the transit time distributions, making it challenging to estimate-quantify how much of the streamwater-actually-is stream water is actually older than 100 days. In addition, weekly-resolution  $\delta^{2}\text{H}$  measurements led to deceptively high-performance metrics (e.g., Nash-Sutcliffe Efficiency), even when key model parameters for groundwater age selection—such as young-versus-old-water selection preferences—remain poorly constrained. As a result, the variation in the estimation of the fraction of stream water younger than 1000 days was approximately days. The variability in streamflow TTD estimates arising from different groundwater SAS function shapes was considerable ( $\pm 20\%$  in the HOAL and for HOAL and  $\pm 23\%$  in the Wüstebach catchments due to the SAS function shape holding similar model performance for Wüstebach), highlighting that TTD estimates are sensitive to how SAS functions are conceptualized and parameterized within the model. These findings underscore the need for complementary data sources, such as multiple tracers, high-frequency sampling, tracer analysis, and/or groundwater-level monitoring, to better constrain preferential flow processes and to reduce uncertainty in catchment-scale water transit time modelling.

## 1 Introduction

Groundwater plays a crucial role in the hydrological cycle and in sustaining streamflow in dry periods, thus regulating the timing and quality of water reaching streams during low-flow periods, and influences the stream water age and quality (van der Velde et al., 2011; Hamilton, 2012; Kaandorp et al., 2018b). The movement of precipitation through the soil matrix into the groundwater and eventually to the stream spans a wide range of timescales: from rapid responses over days to months (Kaandorp et al., 2018a) to slower contributions over years to decades (Visser et al., 2009; Stewart and Morgenstern, 2016; Wang et al., 2025). This variability-The variation in flow timescales across catchments is driven by many factors, including catchment topology and subsurface flow path heterogeneity, which, in turn, leads to spatial and temporal variability in stream water sources and chemical composition (McGuire and McDonnell, 2006; Hamilton, 2012; Kaandorp et al., 2018b). In the light of these complexities, previous studies have long underscored that preferential flow pathways in both partially (Beven and Germann, 1982; Weiler et al., 2003; Klaus et al., 2013) and fully saturated porous media (Bianchi et al., 2011) lead to fast and localised water flow and solute transport, which have the potential to alter stream chemical composition dramatically. Such preferential flow is widely acknowledged in groundwater hydrology (Berkowitz et al., 2006; Hansen and Berkowitz, 2020a; Berkowitz and Zehe, 2020; Hansen and Berkowitz, 2020b; Zehe et al., 2021), and typically referred to as "non-Fickian" or

"anomalous" flow in the groundwater community (Berkowitz and Zehe, 2020; Hansen and Berkowitz, 2020a). While explicitly represented in many dedicated groundwater models (e.g. Berkowitz and Zehe 2020), it remains uncertain whether simpler, top-down catchment-scale, isotope-based transport models can meaningfully ~~detect and quantify~~ represent preferential groundwater flow pathways.

Water molecules entering at different locations ~~of a catchment follow different~~ within a catchment travel along distinct flow paths and take different times to exit the ~~system again~~ catchment via streamflow or evaporation (transit time, TT). The statistical distribution of ~~these~~ transit times is referred to as the transit time distribution (TTD). The transit time of water reflects the key information about how quickly water moves through a ~~catchment control volume, such as catchments~~ (Beven, 2006; Rinaldo et al., 2015; Benettin and Bertuzzo, 2018); hence, how quickly solutes are transported through the surface, subsurface, and eventually to the stream. Despite their usefulness in studying water flow through catchments, TTs cannot be measured directly and are generally inferred using hydrologic models and catchment-wide input-output signals of tracers, such as water stable isotopes ( $\delta^2\text{H}$ ,  $\delta^{18}\text{O}$ ). ~~For the quantification of flow processes and transit times, many~~ Many studies have integrated hydrometeorological data and applied tracer-based modelling, using the TTD to infer flow processes and estimate transit times (e.g., Birkel et al. 2011a; Kuppel et al. 2018; Benettin and Bertuzzo 2018; Harman 2019; Wang et al. 2023). These studies have shown that ~~most water flowing to streams consists of a mixture of multiple~~ streamflow typically consists of water from a broad spectrum of ages, with TTDs spanning ~~timescales~~ from days to decades. ~~The variability in TTDs is influenced by changes~~ aeross space and time (Klaus and McDonnell, 2013; Kirchner, 2016; Wang et al., 2025), thereby highlighting the importance of both rapid transmission of precipitation to streams and its long-term storage in catchments.

In recent years, studies have focused on time-variable transit time distributions by applying the StorAge Selection (SAS) approach (Botter et al., 2011; van der Velde et al., 2012; Hrachowitz et al., 2016; Harman, 2019) ~~combined with catchment scale~~ combined with catchment-scale transport models. The SAS ~~formulation captures the age heterogeneity~~ function represents water age dynamics in hydrological systems by defining the relationship between the distribution of ~~ages stored in the hydrological~~ water ages stored within the system (residence time distribution, RTD) and the ~~ages removed~~ distribution of water ages leaving the system as outflows (transit time distribution, TTD). By applying SAS ~~models~~ functions with multiple functional forms, such as beta (van der Velde et al., 2015), gamma (Harman, 2019), and piecewise linear (Fenicia et al., 2006; McMillan et al., 2012) distributions, and tracking water fluxes, ~~several studies have highlighted the temporal variability of TTDs and demonstrated~~ how studies have shown that TTDs vary over time and that transport processes can differ under varying contrasting conditions, such as between wet and dry periods (Benettin et al., 2015b; Harman, 2015; Kaandorp et al., 2018a). Moreover, using the SAS formulation and ~~conceptualising~~ conceptualizing the catchment as a multi-bucket system, studies have ~~emphasised~~ emphasized the partial age mixing processes of recent precipitation contributing to different fluxes, including evapotranspiration (~~van der Velde et al., 2015; Maxwell et al., 2019~~), (~~van der Velde et al., 2015~~) and macropore flow in the shallow subsurface (~~Hrachowitz et al., 2013; Klaus et al., 2013; Sprenger et al., 2016~~) (~~Hrachowitz et al., 2013~~). This preferential flow of precipitation was found to become more prevalent with increasing soil ~~moisture~~ wetness by bypassing smaller pore volumes and releasing younger water (~~Klaus et al., 2013; Wickenkamp et al., 2016~~) and (~~Klaus et al., 2013~~) or occasionally triggered by high precipitation intensities, leading to overland flow (Türk et al., 2024).

However, despite these findings of partial mixing in the unsaturated zone and the potential of preferential release of young water from groundwater, in many SAS ~~applications the age composition of groundwater flow to the stream is often function~~ applications, the age distribution of baseflow (groundwater contribution to streamflow) is simplified by assuming uniform mixing of stored ages (e.g., Benettin et al. 2015a; Birkel et al. 2015; Ala-Aho et al. 2017; Knighton et al. 2019; Hrachowitz et al. 2013, 2021; Salmon-Monviola et al. 2025), noting that SAS functions are ~~neither straightforward to measure nor not straightforward to~~ parameterize. This simplification is typically adopted i) to maintain model simplicity, ii) due to the lack of robust characterization of subsurface heterogeneity and its induced mixing mechanisms, and iii) due to the limited availability of detailed observations of groundwater flow processes, leaving gaps that must be filled by assumptions such as complete mixing of stored water ages. Nevertheless, several studies have emphasized that TTD estimates depend strongly on the chosen mixing assumptions in SAS models, thereby introducing uncertainty into estimates of transport timescales (van der Velde et al., 2012, 2015; Borriero et al., 2023). Reducing the complexity of groundwater storage representation by employing a single, uniform SAS function shape may, therefore, oversimplify actual groundwater flow processes, potentially leading to erroneous conclusions in the estimation of water transit times.

Indeed, increasing evidence suggests that groundwater systems may not be completely mixed, and ~~the that~~ preferential release of young ~~water groundwater (e.g. recently recharged water) to streams~~ may be a ubiquitous feature of groundwater in heterogeneous aquifers (Berkowitz and Zehe, 2020; Hansen and Berkowitz, 2020a) for several reasons: (i) time-variant hydrological and climatic conditions (Maxwell et al., 2016), (ii) generally low longitudinal and transversal dispersivities in groundwater systems, leading to little mixing, and (iii) complex structural heterogeneities influenced by geology, soil properties, and land use ~~(Janos et al., 2018). for very shallow groundwater (Janos et al., 2018). This evidence suggests that groundwater systems are often not completely mixed, and the preferential release of young water may be common in heterogeneous aquifers.~~ Therefore, SAS functions should ~~reflect that flow processes are transient and that groundwater contributes to the nonlinearity of flow processes and catchment responses (Kaandorp et al., 2018a)~~ be formulated to account for preferential release of young water and the nonlinearities in groundwater contributions and catchment responses.

Furthermore, instead of assuming a single mixed reservoir, and following the conceptualization of Zuber (1986), groundwater is typically described by considering the mixing of active (water that contributes to flow) and passive groundwater storage volumes (water that mixes with the tracer signal of the active water volume but does not contribute directly to flow) (Fenicia et al., 2010; Birkel et al., 2011a; Hrachowitz et al., 2015). Birkel et al. (2011a) emphasised that the presence and extent of the passive storage can significantly influence the interpretation of tracer signals within a catchment. Yet, the extent to which the passive storage volumes and their associated mixing assumptions shape tracer signals and TTD estimations, particularly when combined with different SAS assumptions (e.g., complete mixing vs. partial mixing), still remains to some extent unknown. However, adopting more complex SAS parameterisations with additional parameters may exacerbate model uncertainty, particularly given the limited availability of tracer data to constrain these parameters (Beven, 2006). Consequently, systematically testing different groundwater SAS shapes against long-term tracer observations in streamflow is critical for assessing whether explicitly representing preferential groundwater flow (and associated SAS functions) meaningfully affects the quantification of transit time distributions in catchment-scale isotope-based transport models.

The ~~main~~ objective of this study was to ~~evaluate how variations in SAS function parameterisations for~~ test whether stable  
125 water isotope ( $\delta^2\text{H}$ ) measurements in streamflow can be used within a simple, top-down, catchment-scale transport modeling  
framework to represent preferential flow in the unsaturated root zone and groundwater ~~influence estimated transit times and~~  
~~tracer composition~~, and to assess their influence on transit time distributions. To this end, we evaluated how different parameterizations  
of SAS functions, which describe the release of younger versus older water from storage, affect simulated tracer signals at the  
stream outlet. By systematically comparing ~~the effect of multiple mixing assumptions on the simulation of observed streamflow~~  
130 ~~tracer data~~ multiple parameterizations of SAS functions, we tested the hypothesis that ~~preferential discharge~~ the preferential  
release of young groundwater ~~can be significant and, therefore, should be represented by appropriate SAS functions~~ contributes  
measurably to the streamflow tracer signal and should therefore be represented in catchment-scale transport models. Addi-  
tionally, we examined whether (and how) the extent and mixing assumptions of passive groundwater storage influence the  
interpretation of tracer signals and the estimation of transit times.

135 We specifically addressed the following research questions:

1. *Do precipitation and stream water tracer data have sufficient ~~information content~~ variability to identify and characterize preferential groundwater flow processes using different SAS function shapes, and if so, which SAS functions best represent these processes at the catchment scale?*
- 140 2. *Does explicitly accounting for the preferential release of young water in groundwater ~~flow using different~~, through a ~~SAS functions significantly~~ function, affect catchment-scale transit time distributions and ~~the interpretation of simulated~~ tracer signals in streamflow?*
- 145 3. *~~To~~ How and to what extent ~~does the passive storage volume and associated~~ do different groundwater mixing as-  
sumptions ~~influence the representation of preferential groundwater flow~~, in combination with varying passive storage  
volumes, affect the ~~estimated transit time distributions~~ model's ability to reproduce streamflow tracer signals, and the  
~~interpretation estimation of tracer signals~~ transit time distributions at the catchment scale?*

To answer these questions, we used long-term hydrological and  $\delta^2\text{H}$  data from two contrasting headwater catchments. Each  
site exhibits distinct seasonal variability in ~~runoff stable isotope~~ streamflow  $\delta^2\text{H}$  signatures: one catchment displays minor  
isotopic variations during baseflow and sharp event-based responses (a “flashy” catchment), while the other catchment exhibits  
pronounced isotopic seasonality even during baseflow conditions. We implemented a time-variant TTD modelling framework  
150 capable of representing various mixing scenarios within these catchments.

## 2 Materials and methods

### 2.1 Study sites

The study sites for this study were the Hydrological Open Air Laboratory (HOAL) in Petzenkirchen ([Fig. S 2](#)), Lower  
Austria (Blöschl et al., 2016), and the Wüstebach headwater catchment ([Fig. S 1](#)) in Germany's Eifel National Park ([↗](#))

155 (Bogena et al., 2015). The HOAL covers 66 hectares and features a humid climate with a mean annual air temperature of around 9.5°C. The mean annual precipitation and runoff are approximately 823  $mm\ yr^{-1}$  and 195  $mm\ yr^{-1}$ , respectively. The elevation ranges from 268 to 323 m a.s.l., with a mean slope of 8 %. Predominant soil types in the HOAL catchment include Cambisols (57 %), Planosols (21 %), Kolluvisols (16 %), and Gleysols (6 %). The area's geology consists of Tertiary fine sediments of the Molasse underlain by fractured siltstone. Land use primarily includes agriculture (commonly maize, winter wheat, and rapeseed) (87 %), supplemented by forest (6 %), pasture (5 %), and paved areas (2 %) (Blöschl et al., 2016).  
160 The Wüstebach headwater catchment, part of the Lower Rhine/Eifel Observatory within the TERENO network, covers 38.5 hectares. It is characterized by a humid climate, with an annual temperature of around 7°C, mean annual precipitation of about 1200  $mm\ yr^{-1}$ , and mean annual runoff of 700  $mm\ yr^{-1}$ . The catchment's elevation ranges from 595 to 630 m a.s.l., with gentle hill slopes surrounding a relatively flat riparian area near the stream. The bedrock is primarily Devonian shales, interspersed with sandstone inclusions and overlaid by periglacial layers. The hillslopes predominantly comprise Cambisols, while the riparian area features Gleysols and Histosols. The land use is primarily spruce forest (Bogena et al., 2018).  
165

## 2.2 Hydrological and tracer data

We used daily hydro-meteorological data from October 2013 to 2019 for the HOAL catchment (Fig. 1a, 1b) and from October 2009 to October 2013, for the Wüstebach catchment (Fig. 1c, 1d). For the Wüstebach catchment, partial deforestation in  
170 October 2013 led to changes in catchment-flow-streamflow generation processes (Hrachowitz et al., 2021). Therefore, the period after deforestation was not used for the analyses.

In the HOAL, precipitation data were recorded using a weighing rain gauge located 200 m from the catchment outlet, and stream discharge was measured at the catchment outlet using a calibrated H-flume. The precipitation samples for isotopic analysis were collected using an adapted Manning S-4040 automatic sampler located approximately 300 m south of the catchment.  
175 In addition to precipitation samples, weekly grab samples of streamflow were collected at the catchment outlet for isotopic analysis. Additionally, event-based streamflow samples were collected using an automatic sampler, with the frequency of sampling adjusted based on flow rate thresholds (without exceeding sampling bottle capacity). Isotopic measurements of  $\delta^{18}O$  and  $\delta^2H$  were conducted using cavity ring-down spectroscopy (Picarro L2130-i and L2140-i), with an analytical uncertainty of  $\pm 0.1\ ‰$  for  $\delta^{18}O$  and  $\pm 1.0\ ‰$  for  $\delta^2H$ .

180 ~~Hydrological and tracer data of the HOAL and Wüstebach catchments: (a, c) daily measured streamflow  $Q$  ( $mm\ d^{-1}$ ) and precipitation  $P$  ( $mm\ d^{-1}$ ), (b, d) precipitation  $\delta^2H$  signals (light blue) and streamflow  $\delta^2H$  signals (dark blue); the size of the dots indicates the relative precipitation volume. For the HOAL catchment, the  $\delta^2H$  data of streamflow was further shown as the weekly grab samples (b, dark blue dots) and event samples (b, orange dots). For the HOAL catchment, precipitation  $\delta^2H$  samples are in daily resolution, whereas for the Wüstebach catchment, beginning in September 2012, the sampling frequency for precipitation  $\delta^2H$  increased from weekly to daily (d).~~

In the Wüstebach catchment, precipitation data were obtained from a nearby meteorological station operated by the German Weather Service (Deutscher Wetterdienst, DWD station 3339), and stream discharge was measured using a V-notch weir for low flows and a Parshall flume for high flows (Bogena et al., 2015). The precipitation samples for isotopic analysis were collected

at the Schönesseiffen meteorological station, located approximately 3 km northeast of the catchment at an elevation of 620 m  
190 a.s.l. Starting in June 2009, weekly precipitation samples were collected using a cooled storage rain gauge with 2.3-L HDPE  
bottles (Stockinger et al., 2014). From September 2012 onward, the sampling resolution was increased to daily intervals (Fig.  
1d) using a cooled automated sampler (Eigenbrodt GmbH & Co. KG, Germany; 250 mL PE bottles). Stream water samples  
for isotopic analysis were collected weekly at the catchment outlet as grab samples. Cavity ring-down spectroscopy (Picarro  
L2120-i, L2130-i) was used for water isotope analyses, with an analytical uncertainty of  $\pm 0.1$  ‰ for  $\delta^{18}\text{O}$  and  $\pm 1.0$  ‰ for  
195  $\delta^2\text{H}$ . All isotopic measurements are reported as per mil (‰) relative to Vienna Standard Mean Ocean Water (VSMOW).

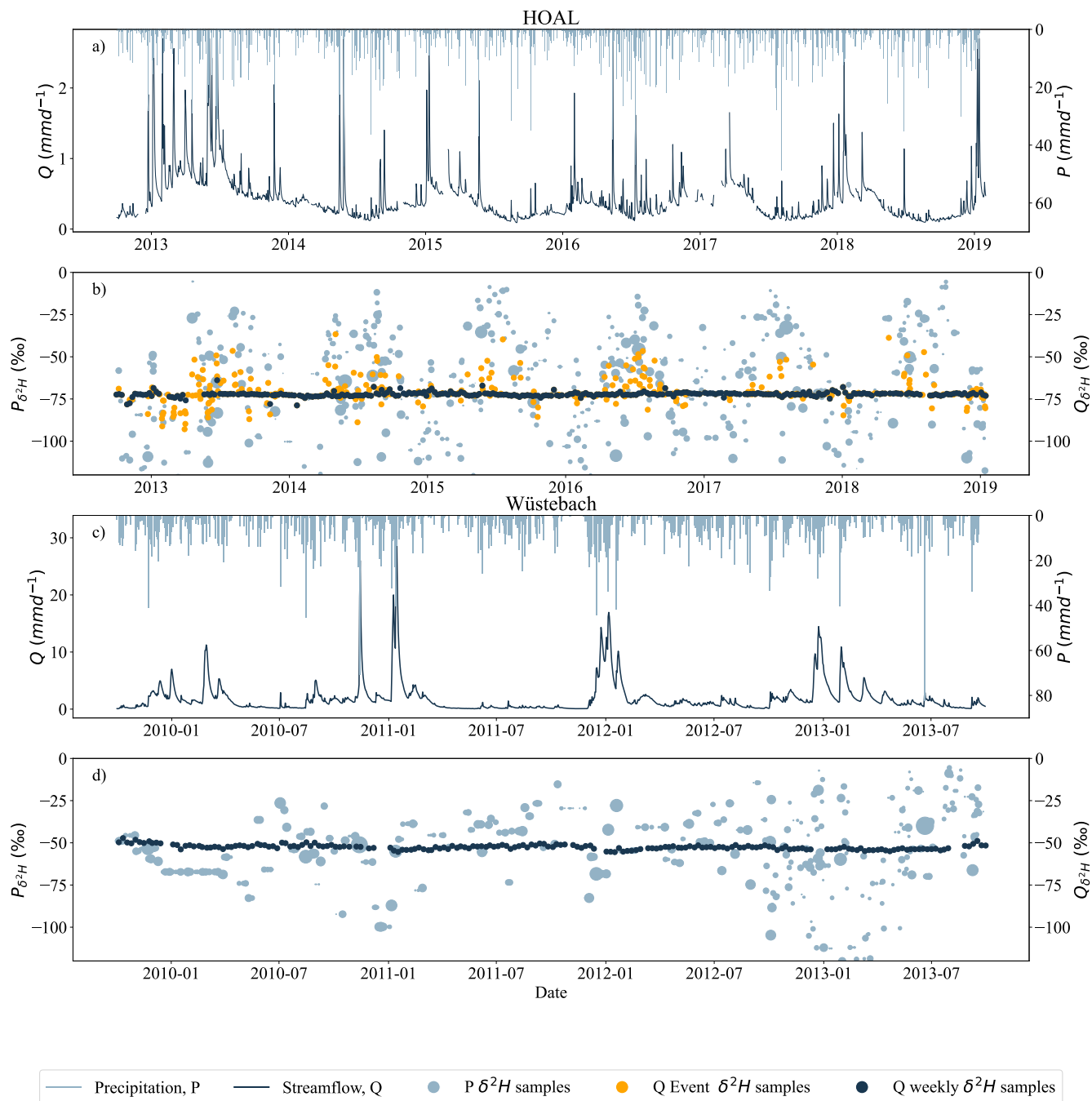


**Figure 1.** Hydrological and tracer data of the HOAL and Wüstebach catchments. (a, c) daily measured streamflow  $Q$  ( $mmd^{-1}$ ) and precipitation  $P$  ( $mmd^{-1}$ ), (b, d) precipitation  $\delta^2H$  signals (light blue) and streamflow  $\delta^2H$  signals (dark blue); the size of the dots indicates the relative precipitation volume. For the HOAL catchment, the  $\delta^2H$  data of streamflow was further shown as the weekly grab samples (b, dark blue dots) and event samples (b, orange dots). For the HOAL catchment, precipitation  $\delta^2H$  samples are in daily resolution, whereas for the Wüstebach catchment, beginning in September 2012, the sampling frequency for precipitation  $\delta^2H$  increased from weekly to daily (d).

### 2.3 Hydrological model and tracer transport model

We used a process-based hydrological and transport model (Türk et al., 2024) based on the DYNAMITE modelling framework (Hrachowitz et al., 2014). Briefly, both the HOAL and Wüstebach catchments are conceptualised through five interconnected reservoirs: snow, canopy interception, unsaturated root zone, fast response storage, and groundwater with active and passive components (Fig. 2). The model hydrological fluxes are: total precipitation  $P$  ( $\text{mm d}^{-1}$ ), precipitation as snow  $P_s$  ( $\text{mm d}^{-1}$ ), precipitation as rain  $P_r$  ( $\text{mm d}^{-1}$ ), snow-melt  $P_m$  ( $\text{mm d}^{-1}$ ), throughfall  $P_e$  ( $\text{mm d}^{-1}$ ), interception evaporation  $E_i$  ( $\text{mm d}^{-1}$ ), evaporation from the root zone  $E_a$  ( $\text{mm d}^{-1}$ ), preferential fast response  $R_f$  ( $\text{mm d}^{-1}$ ), fast preferential recharge to the to groundwater  $R_{fs}$  ( $\text{mm d}^{-1}$ ), preferential fast response  $R_{ff}$  ( $\text{mm d}^{-1}$ ), infiltration-excess overland flow  $Q_o$  ( $\text{mm d}^{-1}$ ), preferential fast response to the fast-responding bucket  $R_{fn}$  ( $\text{mm d}^{-1}$ ), flow from the fast-responding reservoir  $Q_f$  ( $\text{mm d}^{-1}$ ), saturation-excess overland flow from the fast-response bucket  $Q_{of}$  ( $\text{mm d}^{-1}$ ), slow recharge to the groundwater reservoir  $R_s$  ( $\text{mm d}^{-1}$ ), baseflow from the groundwater reservoir  $Q_s$  ( $\text{mm d}^{-1}$ ), deep infiltration loss  $Q_l$  ( $\text{mm d}^{-1}$ ), and the total discharge to the streamflow  $Q_{tot}$  ( $\text{mm d}^{-1}$ ). Model calibration parameters are shown in red adjacent to the model component they are associated with (Fig. 2), and symbols are defined in Table S 2. All model equations are defined in Table S 1

To route  $\delta^2\text{H}$  fluxes through the model, the ~~storage-age-selection function (SAS)~~ SAS approach (Rinaldo et al., 2015; Harman, 2015) was integrated into the hydrological model. ~~This model formulation allows the simulation of water fluxes and tracer dynamics simultaneously, enabling the estimation of TTDs from the age distributions of stored water. The SAS function was formulated as~~ In this integrated framework, each storage defined within the hydrological model (e.g.,  $S_r, S_f$ , Fig. 2), at any given time  $t$ , stores water of different ages, represented as  $T$ , which traces back to past precipitation and is ranked by their input time. The age distribution of a storage at time  $t$  is termed  $p_s(T, t)$ , and is in its cumulative form  $S_T(T, t)$ , also known as the cumulative residence time distribution (RTD). The output fluxes  $O$  ( $\text{mm d}^{-1}$ ) (e.g.,  $E_a, R_s$ , Fig. 2) are subsets of specific ages from the storage with water age distributions termed  $p_{Q,T}(T, t)$ , which are known in their respective cumulative form  $O_T(T, t)$  as cumulative transit time distributions (TTD). The relation between storage and output fluxes is formulated based on the SAS function  $\omega_{Q,m,j}$  that SAS defines the likelihood of selecting water parcels of different ages ~~from catchment storage compartments~~ for release from the storage, thereby translating the internal age structure of the storage into an age distribution of output fluxes. At each time  $t$ , the age-ranked water in storage is characterized by its tracer composition  $C_S(T, t)$ , which reflects the signal of past precipitation inputs. The output fluxes are likewise described by their tracer distributions,  $C_O(T, t)$ , derived from the selection of water ages leaving storage.

Then, the transport balance of the storage is built on water age conservation over time :

$$\frac{\partial S_{T,j}(T, t)}{\partial t} + \frac{\partial S_{T,j}(T, t)}{\partial T} = \sum_{n=1}^N I_{T,n,j}(T, t) - \sum_{m=1}^M O_{T,m,j}(T, t) \quad (1)$$

where:  $\frac{\partial S_T(T, t)}{\partial t}$  is the rate of change of age-ranked storage with respect to time,  $\frac{\partial S_T(T, t)}{\partial T}$  represents the ageing of water within the storage,  $I_{T,n}(T, t)$  are the cumulative age-ranked inflows  $O_{T,m,j}(T, t)$  are the cumulative age-ranked outflows.  $N$  and  $M$  denote the number of inflows and outflows from a given storage component (e.g., ~~unsaturated zone~~) to outputs (e.g.,

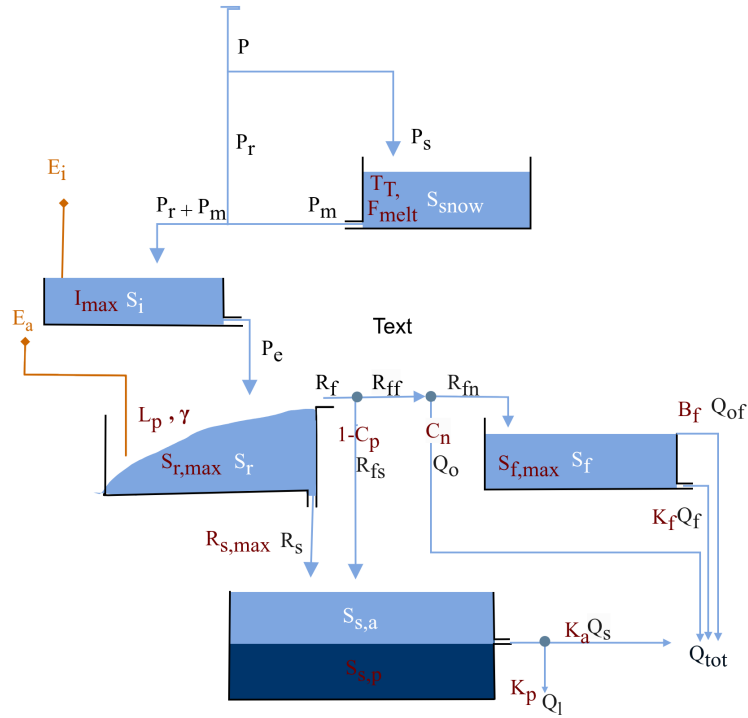


**Figure 2.** The model structure used to represent the HOAL and the Wüstebach catchment (adapted from Türk et al. (2024)). Light blue boxes indicate the hydrologically active storage volumes that contribute to total discharge  $Q_{tot}$ : Snow storage ( $S_{snow}$ ), canopy interception ( $S_i$ ), fast response bucket ( $S_f$ ), root zone storage ( $S_r$ ), and “active” groundwater ( $S_{s,a}$ ). The darker blue box ( $S_{s,p}$ ) indicates a hydrologically “passive” groundwater volume. Blue lines indicate snow and water fluxes, while orange lines indicate water vapour fluxes. Model parameters are shown in red adjacent to the model component they are associated with and symbols are defined in Table S 2. All model equations are defined in Table S 1

streamflow or evapotranspiration) for the root zone, N would be  $P_e$  and M is  $E_a$ ,  $R_f$ , and  $R_s$ ; see Fig.2). Each age-ranked outflow  $O_{T,m,j}(T,t)$  (Eq.2) from a specific storage component  $j$  depends on the cumulative age distribution of that outflow  $P_{O,m,j}(T,t)$  and outflow volume  $O_{m,j}(t)$ , which is estimated by the hydrological balance component of the model.

$$O_{T,m,j}(T,t) = O_{m,j}(t) P_{O,m,j}(T,t), \quad (2)$$

where  $O_{m,j}(t)$  is the total outflow rate, and

$$P_{O,m,j}(T,t) = \Omega_{o,m,j}(S_{T,j}(T,t), t) \quad (3)$$

The cumulative age distribution  $P_{O,m,j}(T,t)$  (Eq.3) is the backward TTD of that outflow in cumulative form and depends on the age-ranked distribution of water in the storage component  $j$  at time  $t$ ,  $S_{T,j}(T,t)$ , and the probability density function, which in this case is the SAS function  $\omega_{O,m,j}$  (or  $O_T(T,t)$  in its cumulative form) of that flux.

From the cumulative age distribution, the associated probability density function can be derived according to

$$p_{o,m,j}(T,t) = \bar{\omega}_{o,m,j}(S_{T,j}(T,t),t) \frac{\partial S_{T,j}(T,t)}{\partial T}, \quad (4)$$

240 where  $\omega_{o,m,j}(S,t)$  is a probability density function of normalized rank storage  $S_{T,\text{norm},j}(T,t)$  (Eq. 5). Normalizing the age-ranked storage  $S_T(T,t)$  by its total volume  $S_j(t)$  binds  $S_{T,\text{norm},j}$  to the interval  $[0,1]$  and holds mass balance without requiring rescaling of the SAS function at each time step.

$$S_{T,\text{norm},j}(T,t) = \frac{S_{T,j}(T,t)}{S_j(t)}, \quad (5)$$

so that  $0 \leq S_{T,\text{norm},j} \leq 1$ .

Finally, the tracer composition of outflow  $m$  from compartment  $j$  is computed as :

$$245 C_{O,m,j}(t) = \int_0^{S_j} C_{S,j}(S_{T,j}(T,t),t) \bar{\omega}_{O,m,j}(S_{T,j}(T,t),t) dS_T \quad (6)$$

where  $C_{O,m,j}(t)$  is the tracer composition in outflow  $m$  from storage component  $j$  at time  $t$ , and  $C_{S,j}$  is the tracer composition in storage at time  $t$ . The model reproduces TTDs for all fluxes and storage components (Fig. 2) at each time step  $t$ . Further details on the model architecture and assumptions can be found in previous studies (Hrachowitz et al., 2014; Fovet et al., 2015). The water balance and flux equations for the two catchments in this study application are described in Türk et al. (2024) and provided in the supplementary Table S 1

250 Similar to previous tracer transport studies for the HOAL (Türk et al., 2024) and Wüstebach (Hrachowitz et al., 2021) catchments, we used beta distributions to formulate the SAS functions. Beta distributions are defined by two shape parameters ( $\alpha$  and  $\beta$ ). For all modelled SAS functions, When both parameters of the Beta distribution were equal to 1 ( $\alpha = \beta = 1$ ), water is uniformly sampled from storage without any preference for specific ages. If  $\alpha < \beta$  (or  $\alpha > \beta$ ), a selection preference for younger (or older) water existed, respectively. To limit the number of model parameters,  $\beta$  was fixed at 1. The time variability of the SAS function shape was then determined by the age-ranked storage and the shape parameter  $\alpha$ , which was bounded between 0 and 1 to represent a preference for younger storage, and greater than 1 to represent a preference for older storage. Preferential release of older water ( $\alpha > 1$ ) decreases the mean residence time of stored water, as older water is removed from storage. Conversely, preferential release of younger water ( $\alpha < 1$ ) increases the mean residence time of stored water, as older water remains stored for longer periods.

260 In principle, the model has 16 outfluxes (Fig. 2), and each of the outflux (e.g.,  $E_a, R_s$ ) requires a separate SAS function parameter  $\alpha$  to be calibrated. However, this is computationally infeasible and would introduce model parameter complexity. Therefore, for all modelled outflows,  $\alpha$  and  $\beta$  were fixed at 1, except those representing preferential flow from the unsaturated

265 root zone (named as  $S_{U,\alpha}$  Table S 2), the  $\alpha$  and  $\beta$  parameters were initially fixed at 1. This ensured uniform sampling of water parcels of different ages from catchment storage compartments into the outflows fixed at 1 for model calibration.

In the Wüstebach catchment, previous studies (Wiekenkamp et al., 2016; Hrachowitz et al., 2021) identified ~~showed that~~ catchment soil wetness ~~as the primary is the main~~ driver for activating preferential flow pathways in the unsaturated zone, ~~leading to the preferential release of young water to the streamflow as soil wetness increases~~. Therefore, the SAS function ~~shape parameter~~ representing preferential flow from the unsaturated root zone ( $R_f$ , Fig. 2) was formulated as a time-variable function of ~~soil wetness to reflect~~ relative soil wetness ( $S_r/S_{r,\max}$ ), where  $S_r$  is the water volume in the root zone at time  $t$ , and  $S_{r,\max}$  is the maximum root-zone storage capacity (calibrated parameter). Equation 8 adopts an increasing probability of young water release with increasing soil wetness through the time-dependent shape parameter  $\alpha(t)$ , reflecting changes in transport processes between wet and dry soil conditions. ~~The temporal variability in the SAS function was implemented through a time-dependent shape parameter  $\alpha(t)$  (Eq. 8).~~

275 In the HOAL catchment, previous studies ~~have~~ highlighted the non-linearity of preferential flow generation ~~in the unsaturated zone~~, where both precipitation intensity and soil ~~moisture influence~~ ~~wetness control~~ the activation of preferential flow pathways (Türk et al., 2024; Széles et al., 2020). ~~To represent this behaviour,~~ (Széles et al., 2020; Vreugdenhil et al., 2022). Overland flow occurs when precipitation exceeds a certain threshold, routing recent precipitation directly to the stream with minimal interaction with stored water (Türk et al., 2024). To account for the combined roles of soil wetness and precipitation intensity ~~in the activation of preferential flow and the release of young water in HOAL catchment, we parameterized~~ the SAS function ~~was formulated with~~ for preferential flow from the unsaturated root zone ( $R_f$ , Fig. 2) using a time-variable shape parameter  ~~$\alpha(t)$ . Here,  $\alpha(t)$  varied~~  $\alpha(t)$  defined as a function of ~~soil moisture, and both~~ soil wetness state and precipitation intensity. Specifically,  $\alpha(t)$  was formulated as a function of relative soil wetness (scaled by the maximum root-zone storage capacity,  $S_{r,\max}$ ) and precipitation intensity ( $P_r/P_I$ ,  $\text{mm d}^{-1}$ ), with a threshold parameter ( $P_{\text{thresh}}$ ) controlling the onset of ~~precipitation-driven preferential flow. This causal formulation was implemented to ensure that  $\alpha(t)$  dynamically responds to both wetness conditions and event-scale precipitation forcing, allowing the model to capture the non-linear activation of preferential flow observed in the catchment. The dual dependence of  $\alpha(t)$  on soil wetness and precipitation intensity, therefore, extends previous SAS applications by providing a more flexible representation of unsaturated zone preferential flow dynamics in HOAL.~~

290 For the HOAL catchment, ~~the~~ time variability of  ~~$\alpha$~~   $\alpha$  for preferential flow in the unsaturated root zone was defined as:

$$\alpha(t) = \begin{cases} \alpha_0, & \text{if } P_r(t) \geq P_{\text{thresh}} \\ 1 - \frac{S_r(t)}{S_{r,\max}}(1 - \alpha_0), & \text{if } P_r(t) < P_{\text{thresh}} \end{cases} \quad (7)$$

For the ~~Wustebach~~ ~~Wüstebach~~ catchment, time variability of  $\alpha$  for the preferential flow in the unsaturated root zone was defined as:

$$\alpha(t) = 1 - \left( \frac{S_r(t)}{S_{r,\max}} \right) (1 - \alpha_0) \quad (8)$$

295 In both Equations 7 and 8, the ~~shape parameter~~ time variable shape parameter  $\alpha(t)$  controls the preferential release of younger water: values of  $0 < \alpha < 1$   $0 < \alpha(t) < 1$  indicate a bias towards younger water parcels, whereas  ~~$\alpha = 1$~~   $\alpha(t) = 1$  corresponds to uniform sampling. The  $\alpha_0$  is a calibration parameter representing the lower bound between 0 and 1, allowing  $\alpha(t)$  to vary between  $\alpha_0$  and 1. When soil ~~moisture wetness~~ is low ( $S_r(t) \ll S_{r,max}$ ),  $\alpha(t)$  approaches 1, indicating uniform sampling. As soil ~~moisture wetness~~ increases ( $S_r(t)$  approaches  $S_{r,max}$ ),  $\alpha(t)$  decreases towards  $\alpha_0$ , reflecting a stronger preference  
300 for younger water. In Equation 7, the lower bound  $\alpha_0$  is applied directly whenever precipitation intensity exceeds a certain threshold ( $P_{thresh}$ ).

### 2.3.1 Model calibration and evaluation

We used daily time steps in the model parameter calibration for the period from October 2014 to 2019 for the HOAL catchment and for the period from October 2010 to October 2013 for the Wüstebach catchment to simulate streamflow  $Q$  ( $mm\ d^{-1}$ ) and  
305  $\delta^2H$  signature. The model warm-up period was one year for both catchments; i.e., from October 2013 to October 2014 for the HOAL catchment, and from October 2009 to October 2010 for the Wüstebach catchment.

For model parameter optimization, we used the Differential Evolution algorithm (Storn and Price, 1997) and an objective function that combined five performance criteria related to streamflow and  $\delta^2H$  dynamics. The objective function included the Nash-Sutcliffe efficiencies (NSE) of streamflow (to evaluate overall discharge dynamics), logarithmic streamflow (to match  
310 low-flow conditions), the flow duration curve (to capture the distribution of flows over time), the runoff coefficient averaged over three months (to ensure water balance consistency), and the NSE of the  $\delta^2H$  signal in streamflow (to constrain  $\delta^2H$  dynamics) (Table S 3). These individual performance metrics were aggregated into the Euclidean distance  $D_E$  ~~to the perfect model~~, with equal weights assigned to streamflow and the  $\delta^2H$  signature, according to:

$$D_E = \sqrt{\frac{1}{2} \left( \frac{\sum_{i=m}^M (1 - E_{Q,m})^2}{M} + \frac{\sum_{i=n}^N (1 - E_{18O,n})^2}{N} \right)} \quad (9)$$

315 Where  $M = 4$  is the number of performance metrics with respect to streamflow,  $N = 1$  is the number of performance metrics for tracers ~~in each combination~~, and  $E$  is the evaluation matrix based on goodness-of-fit criteria. The Euclidean distance  $D_E$  to the ~~“perfect optimal~~ model” (where  $D_E = 0$  indicates a perfect fit) was used to ensure that overall model performance remained balanced. Only solutions achieving  $D_E \leq 1$  were accepted as feasible solutions for further analysis. The accepted solutions were then ranked in order of decreasing  $D_E$ , and the solution with the lowest  $D_E$  was selected as the ~~optimal~~-parameter  
320 set for TTD estimations. Transit times were estimated up to a tracking period of 1000 days, limited by data availability, and the mean of the estimated TTD was compared between dry periods (streamflow below the 25<sup>th</sup> percentile,  $Q_{25}$ ) and wet periods (streamflow above the 75<sup>th</sup> percentile,  $Q_{75}$ ). In addition, the young-water fraction of daily streamflow ( $F_{Q(T < 90)}$ ) was calculated as the sum of streamflow fractions with transit times up to 90 days. Its monthly variability was then analyzed in relation to the corresponding monthly variability of soil wetness ( $\frac{S_r}{S_{r,max}}$ ) for both catchments.

### 325 2.3.2 Sensitivity test of root zone and groundwater SAS functions

~~To evaluate whether precipitation and stream water tracer data carry sufficient information to identify preferential flow paths, and to examine how different groundwater SAS function shapes might affect catchment-scale transit time distributions, we conducted a stepwise analysis (Fig. 3). In this approach, the model was run with calibrated hydrological parameters with different configurations for the~~ In this analysis, we systematically tested the sensitivity of the streamflow  $\delta^2\text{H}$  signal simulations and inferred transit times to changes in the StorAge Selection (SAS) function shape parameter  $\alpha_0$  in parameterization for both the unsaturated root zone and  $\alpha$  the groundwater compartments. ~~To identify if variations in transit time distributions were solely due to differences in age selection formulated by StorAge Selection (SAS), we kept all other hydrological parameters constant across scenarios. By using the same calibrated parameters (e.g., maximum percolation rate, storage capacities, and flow path configurations) for HOAL and Wüstebach in each scenario, any differences in the simulated age distributions can then be~~ attributed to the changes in the SAS function formulation. We first tested the sensitivity of the  $\delta^2\text{H}$  signal to changes in the root zone's streamflow  $\delta^2\text{H}$  signal to root-zone preferential flow by setting systematically varying the lower bound of the SAS shape parameter  $\alpha_0$  to across four values: 0.1 (very young-water preference), 0.7 (young-water preference), 1.0 (uniform selection), and 5.0 (older-water preference), while keeping the groundwater SAS function uniform (i.e.,  $\alpha = 1$ ; Fig. 3a). This approach assesses whether different parametrizations of the SAS function for root-zone preferential pathways alone could reveal a strong impact on the simulated streamflow  $\delta^2\text{H}$  time series and the inferred transit times. Next, we tested the sensitivity of the  $\delta^2\text{H}$  signal to changes in the groundwater SAS function (Fig. 3b) by varying  $\alpha$  across the same range—0.1, 0.7, 1.0, and 5.0—while fixing the previously calibrated optimized  $\alpha_0$  value for the root-zone root-zone preferential flow. This second test was designed to show if (and how) preferential groundwater flow influences different parametrizations of the SAS function for groundwater flow influence the simulated streamflow  $\delta^2\text{H}$  and time series transit time distributions and tracer simulations. ~~At each step, we~~ We evaluated the model's performance in simulating  $\delta^2\text{H}$  using Spearman rank correlation,  $\text{NSE}_{\delta^2\text{H}}$ , and  $\text{MAE}_{\delta^2\text{H}}$ . ~~We then~~ Finally, we calculated daily cumulative TTDs and compared how the mean of these cumulative TTDs their means changed across all scenarios ~~to quantify the impact of SAS function shape on modeled water age distributions. It should be noted that the SAS formulation can only indicate whether preferential release of young water occurs. It does not capture the physical processes driving this behavior, such as soil hydraulic properties, macropore flow, or transient groundwater connectivity.~~

To isolate the effect of the SAS function shape on the simulated streamflow  $\delta^2\text{H}$  signal and on the estimated transit time distributions (TTDs), all hydrological model parameters (e.g., maximum percolation rate, storage capacities, and flow path configurations) were kept identical to the individually calibrated values for the HOAL and Wüstebach catchments. By using the same calibrated parameters while testing different SAS parameterizations for HOAL and Wüstebach, any differences in the simulated  $\delta^2\text{H}$  signals or TTDs can therefore be attributed solely to changes in the SAS function parameterization.

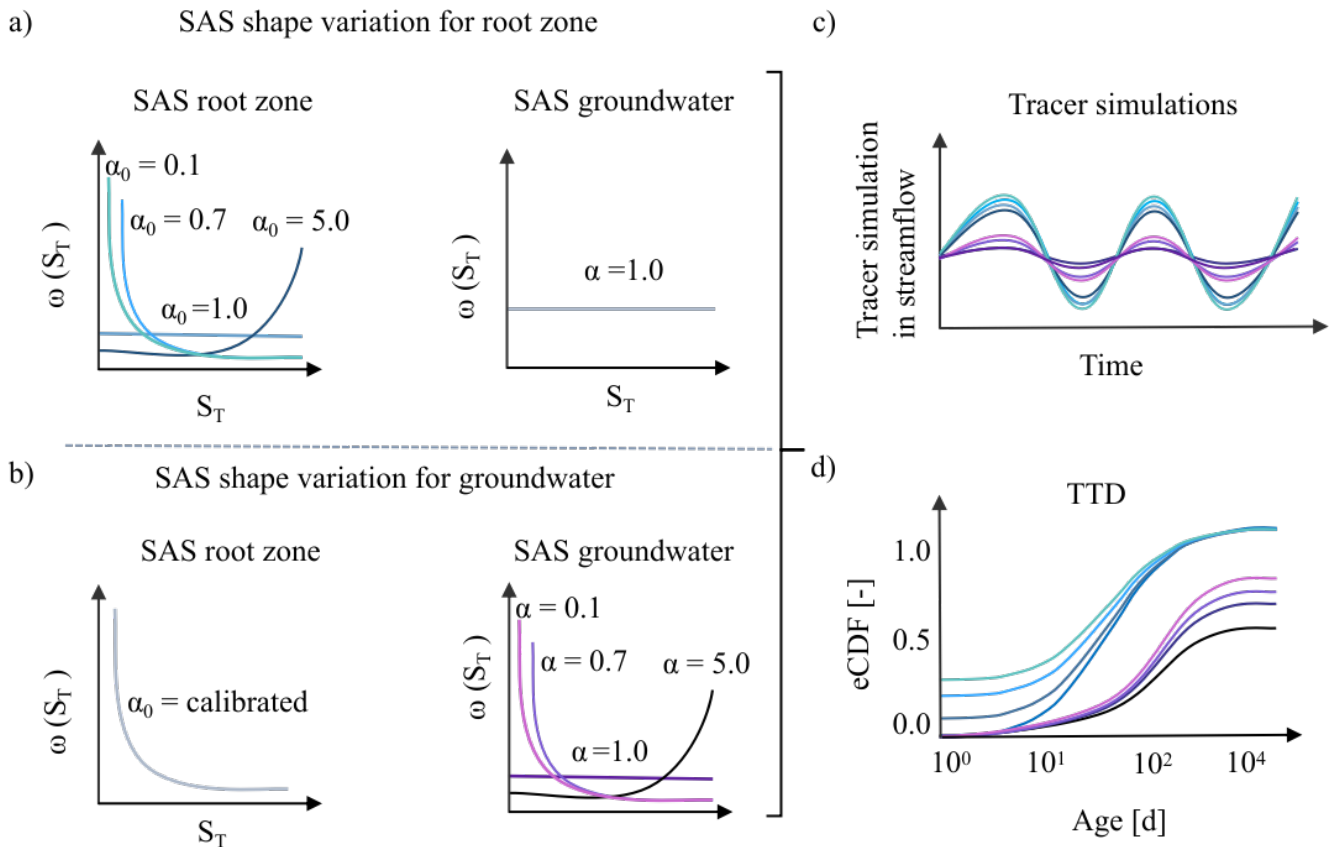


**Figure 3.** Conceptual representation of the stepwise analysis, showing illustrating how different SAS functions, formulated with shape parameter the lower bound  $\alpha_0$  in of the root-zone shape parameter  $\alpha_0$  for root-zone preferential flow and ( $\alpha$ ) for groundwater, flow impact, affect the simulated tracer signals and inferred transit time distributions (TTDs). (a, b) The top-plots illustrate how the unsaturated root-zone SAS function varies with  $\alpha$ . Values of  $\alpha < 1$  indicate a stronger shape parameter  $\alpha_0$  is varied from 0.1 (strong young-water preference for younger water, light blue line) to 5.0 (old-water preference, dark blue line), whereas  $\alpha > 1$  implies preferential release of older water while the groundwater age selection remains uniform. (red-b) The root-zone SAS function shape parameter  $\alpha_0$  is fixed at its calibrated value, and the groundwater  $\alpha$  is varied from 0.1 (strong young-water preference, light purple line) to 5.0 (old-water preference, dark purple line). (a, b) The x-axis,  $S_T$ , represents the age-ranked storage, and the y-axis,  $\omega(S_T)$ , is denotes the relative probability of releasing water of that age. The lower-plots illustrate (c, d) Illustrate the modelled-modeled tracer time series and based on the resulting cumulative transit time distribution. scenarios implemented in (a) The root-zone  $\alpha_0$  is varied from 0.1 and (very young water preference) to 5.0 (older-water preference) while the groundwater compartment remains uniform; (b) the root zone SAS function  $\alpha_0$  is assigned to its calibrated value, and the groundwater  $\alpha$  is varied from 0.1 (very young water preference) to 5.0 (older-water preference) corresponding empirical cumulative transit time distributions.

## 355 2.4 Passive groundwater storage volumes and mixing assumptions with the active groundwater storage

To test In this analysis, we tested whether and to what extent the mixing of the passive groundwater storage with the active groundwater modulates the  $\delta^2\text{H}$  signal in streamflow—and, consequently, influences model performance and inferred transit times—we. We extended the stepwise analysis (Fig. 3b) by varying passive storage volumes (Fig. 4). We used the calibrated SAS function shape parameter ( $\alpha_0$ ) for the root zone preferential flow in combination with In the model setup, groundwater storage was represented as an active component ( $S_{s,a}$ ) and a hydrologically passive component ( $S_{s,p}$ , mm). The passive storage ( $S_{s,p}$ ) does not contribute to baseflow quantity but isotopically mixes with the water of active storage, as illustrated in Figure 2. For the SAS function, the total groundwater storage was defined as the sum of both components ( $S_{s,\text{tot}} = S_{s,a} + S_{s,p}$ ). Consequently, the age-ranked total groundwater storage ( $S_{s,\text{tot}}$ ) represents the combined influence of active and passive storage on the age composition of baseflow ( $Q_s$ , Fig. 2).

### Passive–active groundwater mixing

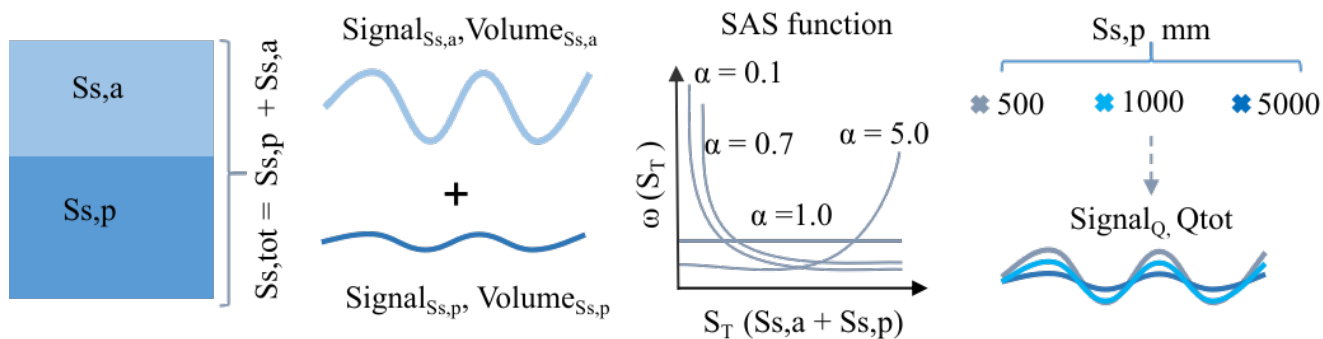


**Figure 4.** Conceptual representation of the analysis illustrating how different passive storage volumes ( $S_{s,p} = 500, 1000,$  and  $5000$  mm) interact with the active storage volume ( $S_{s,a}$ ) under various groundwater SAS function shapes affecting tracer simulations in streamflow. The groundwater SAS function parameter  $\alpha$  is varied from 0.1 (strong young-water preference) to 5.0 (old-water preference). For the SAS function, the x-axis,  $S_T$ , represents the age-ranked total groundwater storage, and the y-axis,  $\omega(S_T)$ , denotes the relative probability of releasing water of that age.

365 We applied three different passive storage volumes ( $S_{s,p} = 500$  mm, 1000 mm, and 5000 mm) to cover the ranges reported for comparable headwater catchments (Birkel et al., 2011a; Benettin et al., 2015a; Hrachowitz et al., 2021). To isolate the effect of passive storage and age-selection parameterization on streamflow  $\delta^2\text{H}$  dynamics and TTD estimations, we kept all hydrological model parameters (e.g., maximum percolation rate, storage capacities, and flow path configurations) identical to the individually calibrated values for the HOAL and Wüstebach catchments. Similar to Figure 3b, four different groundwater mixing scenarios SAS parameterizations were tested (Fig. 4): a strong preference for younger water ( $\alpha = 0.1$ ), a preference for younger water ( $\alpha = 0.7$ ), uniform selection ( $\alpha = 1.0$ ), and a preference for older water ( $\alpha = 5.0$ ) (Fig. 4 a). These scenarios were each

applied to three different passive storage volumes  $S_{s,p} = 500 \text{ mm}, 1000 \text{ mm}, \text{ and } 5000 \text{ mm}$ . We evaluated model performance in simulating streamflow  $\delta^2\text{H}$  by comparing measured and modeled isotope signals using  $\text{NSE}_{\delta^2\text{H}}$  and  $\text{MAE}_{\delta^2\text{H}}$ . To further compare the inferred transit time distributions (TTDs) in each scenario (Fig. 4b)  $\text{NSE}_{\delta^2\text{H}}$  and  $\text{MAE}_{\delta^2\text{H}}$ . In addition, we calculated daily cumulative TTDs and assessed how the mean compared the means of these distributions changed as across different passive storage volumes and mixing assumptions varied SAS parameterizations.

Comparative analysis illustrating how different passive storage volumes ( $S_{s,p}$ : 500 mm, 1000 mm, 5000 mm) mix with the active storage volume ( $S_{s,a}$ ) under various SAS function shapes for groundwater. (a) The root-zone SAS function  $\alpha_0$  is set to its calibrated value, and the groundwater  $\alpha$  is varied from 0.1 (very young-water preference) to 5.0 (older-water preference). Values of  $\alpha < 1$  indicate a stronger preference for younger water (blue line), whereas  $\alpha > 1$  implies preferential release of older water (red line). The x-axis,  $S_T$ , represents the age-ranked storage, and the y-axis,  $\omega(S_T)$ , is the relative probability of releasing water of that age; (b) shows the modelled tracer time series and the resulting cumulative transit time distribution.

### 3 Results

#### 3.1 Variation of $\delta^2\text{H}$ in precipitation and streamflow

In the HOAL catchment,  $\delta^2\text{H}$  values in precipitation ranged from  $-3.0 \text{ ‰}$  to  $-150.0 \text{ ‰}$  (Fig. 1b), with a volume-weighted mean of  $-67.7 \text{ ‰} \pm 31.9 \text{ ‰}$ . Event-based streamflow  $\delta^2\text{H}$  samples ranged from  $-26.2 \text{ ‰}$  to  $-108.0 \text{ ‰}$  (Fig. 1b), while weekly streamflow  $\delta^2\text{H}$  samples ranged from  $-73.2 \text{ ‰}$  to  $-75.2 \text{ ‰}$ . The overall volume-weighted mean of stream samples was  $-71.6 \text{ ‰} \pm 6.1 \text{ ‰}$ .

In the Wüstebach catchment,  $\delta^2\text{H}$  values in precipitation ranged from  $-4.3 \text{ ‰}$  to  $-163.2 \text{ ‰}$  (Fig. 1d, light blue dots), with a volume-weighted mean of  $-52.2 \text{ ‰} \pm 21.4 \text{ ‰}$ . Weekly streamflow  $\delta^2\text{H}$  values exhibited smaller variations, ranging from  $-45.6 \text{ ‰}$  to  $-57.1 \text{ ‰}$  (Fig. 1d). The volume-weighted mean of stream samples was  $-53.2 \text{ ‰} \pm 1.4 \text{ ‰}$ .

Overall,  $\delta^2\text{H}$  in precipitation exhibited large variability in both catchments; however, this signal was attenuated in streamflow. In the HOAL catchment, event-based streamflow  $\delta^2\text{H}$  samples reflected how precipitation inputs were rapidly transmitted to the stream, whereas weekly samples alone would have masked this variability. This highlights the importance of event-based sampling for detecting preferential flow signals, which may remain obscured with weekly data alone. This applies to the Wüstebach catchment, where only weekly streamflow  $\delta^2\text{H}$  measurements were available, which may have prevented the detection of such rapid responses.

#### 3.2 Model calibration

Model calibration resulted in 55 feasible (acceptable model performance with  $\text{DE} < 1$ ) parameter solutions for HOAL (Fig. S 3) and 190 feasible parameter solutions for the Wüstebach catchment (Fig. S 4). The model reproduced the main features of the hydrograph and captured both the timing and magnitude of high and low flow events for the simulation period from October 2014 to 2019 for HOAL (Fig. S 5a, d) and from October 2010 to October 2013 for the Wüstebach catchment (Fig. S 5e, h).

For the HOAL catchment, the mean Nash-Sutcliffe efficiency of streamflow ( $NSE_Q$ ) for the 55 solutions was 0.60 (Fig. S 6). Minor dissimilarities occurred during the spring of 2016, when low flows were overestimated (Fig. S 5a). Nevertheless, the  
405 model simulated most other observed flow signatures reasonably well (Fig. S 6). Among the 55 solutions, the mean NSE for low flows ( $NSE_{\log Q}$ ) was 0.65, for the flow duration curve ( $NSE_{FDC}$ ) was 0.53, and for the three-month averaged runoff ratio ( $NSE_{RC}$ ) it was 0.85. For several rain events, the model captured  $\delta^2H$  fluctuations during high flows and maintained a stable  $\delta^2H$  signal during low flows, with a mean  $NSE_{\delta^2H}$  of 0.51. Overall, the Euclidean distance ( $D_E$ ) for these 55 solutions ranged from 0.60 to 0.33 (Fig. S 6).

410 For the Wüstebach catchment, the mean ~~Nash-Sutcliffe efficiency~~ NSE of streamflow ( $NSE_Q$ ) for the 190 solutions was 0.78 (Fig. S 6). Minor dissimilarities occurred during the spring of 2012, when low flows were overestimated, and the winter of 2012, when peak flows were underestimated (Fig. S 5e). Among the 190 solutions, the mean NSE for low flows ( $NSE_{\log Q}$ ) was 0.65, for the flow duration curve ( $NSE_{FDC}$ ) it was 0.93, and for the three-month averaged runoff ratio ( $NSE_{RC}$ ) it was 0.91. For several rain events, the model captured  $\delta^2H$  fluctuations during high flows and maintained a stable  $\delta^2H$  signal during low  
415 flows, with a mean  $NSE_{\delta^2H}$  of 0.58. Overall, the Euclidean distance ( $D_E$ ) for these 190 solutions ranged from 0.62 to 0.32 (Fig. S 6).

### 3.3 ~~Catchment~~ Modeled catchment transit times

Figure 5 presents the transit time distributions (TTDs) estimated from the initial model calibration, conducted prior to the stepwise experiments. For TTD estimations, we used the model-calibrated parameter set that yielded the lowest  $D_E$ . The results presented hereafter are conditional on the underlying model assumptions and should be interpreted in light of the associated uncertainties.  
420

In the HOAL catchment, the fraction of streamflow younger than 1000 days exhibited considerable variability, ranging from 5 % to 50 % (Fig. 5a). The mean fraction of discharge younger than 1000 days was 13 %; it increased to 15 % during wet periods and decreased to 10 % during dry periods (Fig. 5a). The value of the fraction of streamflow younger than 90 days,  
425  $F_Q(T < 90 \text{ days})$ , varied widely within the same calendar month, ranging from 2 % to 45 %; however, the mean  $F_Q(T < 90 \text{ days})$  across months did not exhibit pronounced seasonal patterns (Fig. 5b). The mean value of simulated relative soil saturation ( $S_r/S_{r,\max}$ ) varied from 0.25 to 0.60 (Fig. 5c).

In the Wüstebach catchment, the mean fraction of discharge younger than 1000 days was 27 %, increasing to 35 % during wet periods and decreasing to 20 % during dry periods (Fig. 5d). The value of the fraction of streamflow younger than 90 days,  
430  $F_Q(T < 90 \text{ days})$  within the same ~~month~~ calendar month ranged between 5 % and 30 % (Fig. 5e), with mean values exhibiting seasonal patterns. The monthly mean of simulated relative soil saturation ( $S_r/S_{r,\max}$ ) ranged from approximately 0.60 to 0.98 (Fig. 5f).

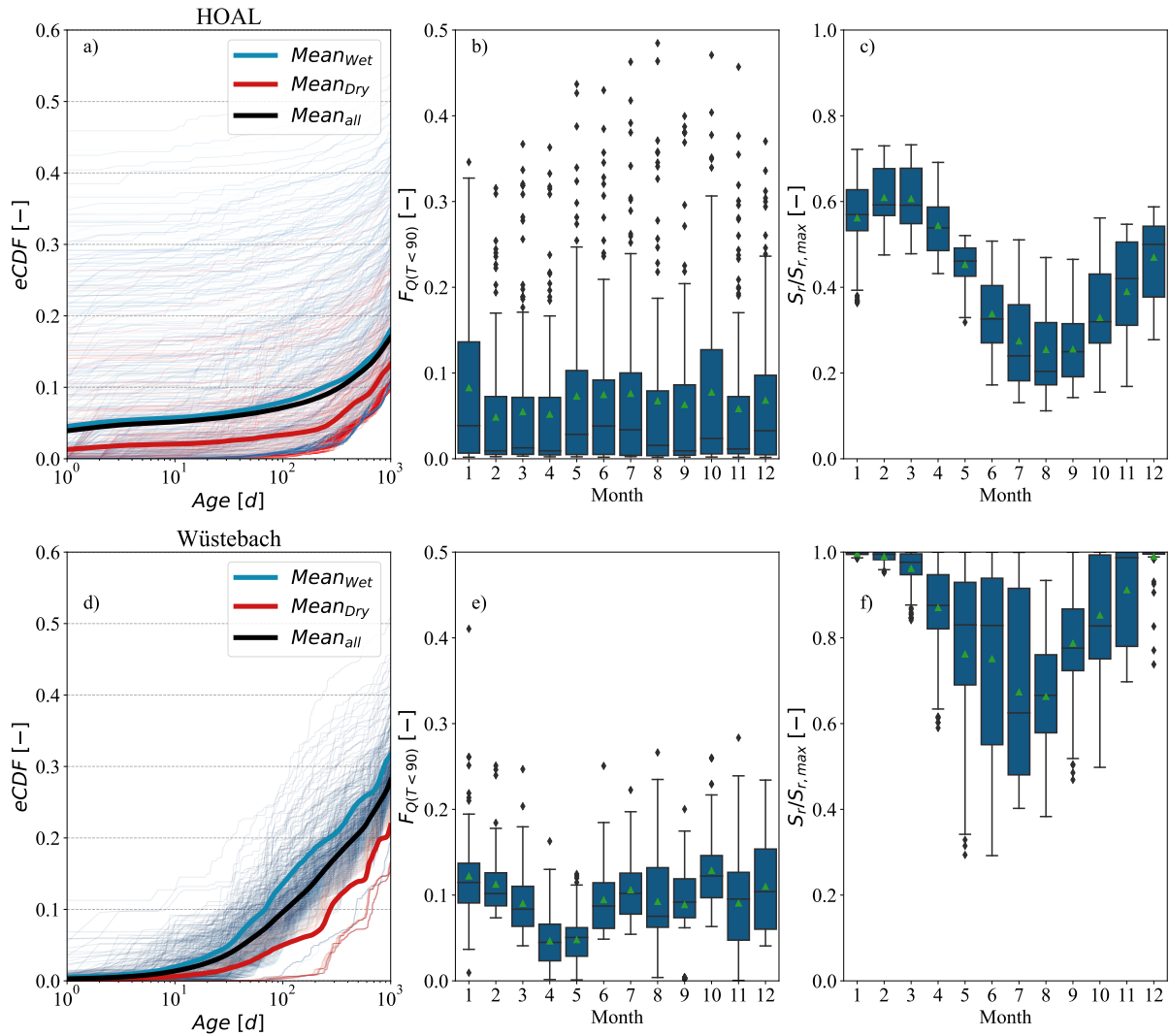


**Figure 5.** Modelled empirical cumulative transit time distributions (TTDs) for daily streamflow in the (a) HOAL and (d) Wüstebach catchments. The colour of the lines corresponds to the wetness state, where dark blue indicates a wet period and dark red indicates a dry period. In panels (a) and (d), the mean of the empirical cumulative TTDs is shown for the entire tracking period (black line), the dry period (red line), and the wet period (dark blue line). The fraction of streamflow younger than 90 days,  $F_Q(T < 90)$ , grouped by month of the year, is shown in panels (b) and (e) for the HOAL and Wüstebach catchments, respectively. Simulated relative soil wetness  $\left(\frac{S_r}{S_{r,max}}\right)$ , also grouped by month of the year, is shown in panels (c) and (f) for the HOAL and Wüstebach catchments, respectively. [Green triangles in panels b, c, e, and f](#) [Green triangles indicate show](#) the mean values.

### 3.4 Sensitivity of $\delta^2\text{H}$ simulations and TTD estimation to different SAS functions in the root zone

In the HOAL catchment, the calibrated root-zone SAS shape parameter lower bound  ~~$\alpha_0 = 0.14$~~  ( $\alpha_0 = 0.14$ ) indicated a strong preference for very young water through unsaturated ~~root-zone-root-zone~~ preferential flow pathways, ~~suggesting that precipitation rapidly reached~~. These reflected the SAS formulation (Eq. 7) on the dual dependence of  $\alpha(t)$  on soil wetness and precipitation intensity. Under high-intensity precipitation,  $\alpha(t)$  takes a value of 0.14, indicating that rapid activation of preferential pathways occurs, allowing precipitation inputs to reach the stream with minimal mixing with stored water. In ~~the contrast, under wetter antecedent conditions,  $\alpha(t)$  increases toward 1, indicating greater mixing within the root zone and contributions of relatively older (i.e., older than recent precipitation inputs) water to streamflow.~~

~~In the~~ Wüstebach catchment, the calibrated SAS shape parameter lower bound  ~~$\alpha_0 = 0.98$~~  suggested ( $\alpha_0 = 0.98$ ) suggested only a slight preference for young water ~~in the root zone's preferential flows~~. Here,  $\alpha(t)$  varied between 0.98 and 1 depending on the soil wetness state (Eq. 8). Under wetter antecedent conditions, established preferential flow pathways facilitated more mixing compared to overland flow, leading to relatively older (i.e., older than recent precipitation) water contributions.

For both catchments, root-zone preferential flow SAS functions ranging from a strong young water preference ( $\alpha_0 = 0.1$ ) to uniform sampling ( $\alpha_0 = 1.0$ ) produced high (positive) Spearman rank correlations ( $r$ ) between modeled and observed  $\delta^2\text{H}$ . In contrast, an old-water preference ( $\alpha_0 = 5.0$ ) yielded negative or weak correlations, indicating a poor fit to the observed tracer signals. In HOAL, the  $r$  values ranged between 0.58, and  $-0.18$  for values of  $\alpha_0$  between ~~0.1~~ and 5.0 (Fig. 6a). The corresponding Nash–Sutcliffe efficiencies ( $\text{NSE}_{\delta^2\text{H}}$ ) ranged between 0.56, and  $-0.25$  (Table 1). In Wüstebach, the  $r$  values for simulated  $\delta^2\text{H}$  ranged between 0.58, and 0.28 for values of  $\alpha_0$  between ~~0.1~~ and 5.0 (Fig. 6b). The corresponding  $\text{NSE}_{\delta^2\text{H}}$  ranged ~~between  $-0.14$ , and~~ ~~betwe~~ 0.51 ~~and  $-0.14$~~  (Table 1).

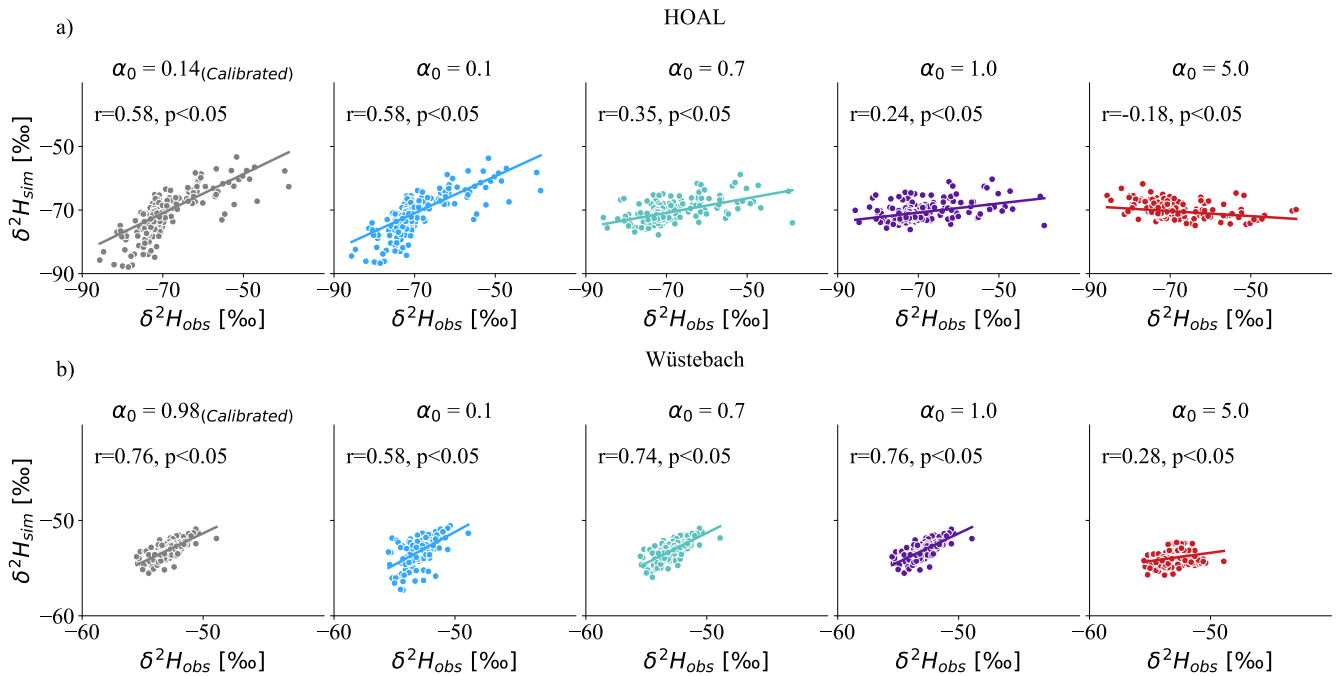


**Figure 6.** Spearman rank correlations between simulated (y-axis) and observed (x-axis)  $\delta^2\text{H}$  signals in streamflow based on varying the SAS shape parameter  $\alpha$  [-] in the root zone for (a) HOAL and (b) Wüstebach. The simulations range from very young preference ( $\alpha = 0.1$ ) to old water preference ( $\alpha = 5.0$ ) for the unsaturated root zone preferential flow, while the groundwater flow was uniformly sampled ( $\alpha = 1$ ).

The Spearman rank correlations ( $r$ ) between observed and simulated  $\delta^2\text{H}$  were lower in HOAL compared to Wüstebach, which can be attributed in part to differences in temporal resolution and the variability of isotope sampling. In HOAL, streamflow  $\delta^2\text{H}$  was sampled on an event basis, with values ranging from  $-26.2\text{‰}$  to  $-108.0\text{‰}$  (Fig. 1b). In contrast, the Wüstebach catchment weekly to biweekly sampling scheme yielded streamflow  $\delta^2\text{H}$  values between  $-45.6\text{‰}$  and  $-57.1\text{‰}$  (Fig. 1b).

455 For both catchments, root-zone preferential flow SAS functions from a preference for young water ( $\alpha_0 = 0.1$ ) to old water ( $\alpha_0 = 5.0$ ) influenced the TTD for ages up to 300 days ( $T < 300$ ). This was due to the fact that is consistent with root-zone storage residence time remained predominantly younger times being predominantly shorter than 300 days (Fig. S 7a, c). Consequently, increasing  $\alpha_0$  from 0.1 to 5.0 and thus reducing the relative contribution of younger flows (Fig. 7a, b),

460 shifted the empirical cumulative distribution functions (eCDFs) toward older water within the first 300 days. In the HOAL, the mean fraction of streamflow with  $T < 300$  days reached about 10% (Fig. 7a,) for all root-zone SAS formulations, whereas in Wüstebach, it was about 20% (Fig. 7b). Overall, these results indicated that root-zone SAS functions with young-water preferences improved the fit to observed streamflow isotopes, highlighting the importance of preferential flow pathways in shaping short transit times and streams  $\delta^2\text{H}$  interpretations.

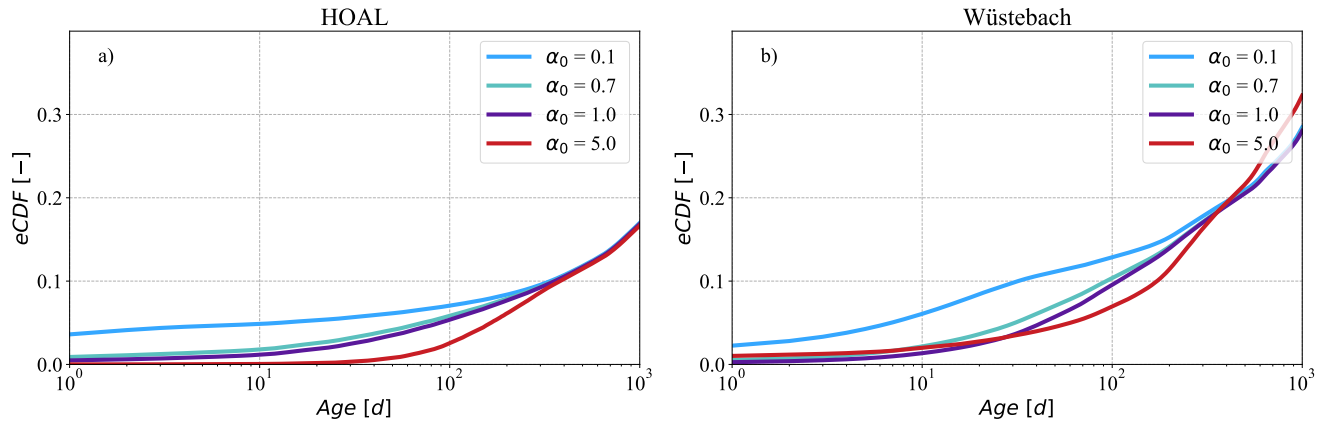


**Figure 7.** The mean of empirical cumulative distribution functions (eCDFs) of simulated transit times of daily discharge for the (a) HOAL and (b) Wüstebach catchments under varying SAS shape parameters in the unsaturated root zone ( $\alpha_0 = 0.1, 0.7, 1.0, 5.0$ ). (a,b) The simulations range from very young preference ( $\alpha_0 = 0.1$ ) to old water preference ( $\alpha_0 = 5$ ) for the unsaturated root zone preferential flow, while the groundwater flow was uniformly sampled ( $\alpha = 1$ ).

**Table 1.** Performance metrics for  $\delta^{2H}$  simulation results under various SAS parameter scenarios for the HOAL and Wüstebach catchments. The table includes the Nash- Sutcliffe efficiency ( $NSE_{\delta^{2H}}$ ) and mean absolute error ( $MAE_{\delta^{2H}}$ ), and Spearman rank correlation coefficients ( $r_{\delta^{2H}}$ ) based on SAS shape parameters ( $\alpha_0$ ) variations in the root zone and groundwater SAS shape parameters ( $\alpha$ ). Scenarios tested represent preferences for very young water ( $\alpha = 0.1$ ), young water ( $\alpha = 0.7$ ), uniform selection ( $\alpha = 1.0$ ), and old water ( $\alpha = 5.0$ ). For simulations testing SAS function variations in the root zone, the groundwater SAS function was kept uniform. Conversely, when testing groundwater SAS function variations, the root zone compartment was assigned its calibrated shape factor ( $\alpha_0 = 0.14$  for HOAL and  $\alpha_0 = 0.98$  for Wüstebach).

Catchment	Metric	SAS Variation: Root Zone				SAS Variation: Groundwater			
		$\alpha_0 = 0.1$	$\alpha_0 = 0.7$	$\alpha_0 = 1.0$	$\alpha_0 = 5.0$	$\alpha = 0.1$	$\alpha = 0.7$	$\alpha = 1.0$	$\alpha = 5.0$
HOAL	$NSE_{\delta^{2H}}$	0.56	0.28	0.15	-0.25	-0.83	0.55	0.56	0.55
	$MAE_{\delta^{2H}}$	2.46	2.85	3.06	4.02	4.75	2.54	2.48	2.48
	$r_{\delta^{2H}}$	0.55	0.35	0.24	-0.18	0.54	0.55	0.56	0.56
Wüstebach	$NSE_{\delta^{2H}}$	-0.14	0.47	0.51	-0.81	0.10	0.05	0.51	0.19
	$MAE_{\delta^{2H}}$	0.90	0.64	0.61	1.14	0.74	0.91	0.61	0.83
	$r_{\delta^{2H}}$	0.58	0.74	0.76	0.28	0.74	0.71	0.76	0.75

### 465 3.5 Sensitivity of $\delta^{2H}$ simulation and TTD estimation to different SAS functions for groundwater

The Spearman rank correlation coefficients ( $r$ ) between simulated and observed  $\delta^{2H}$  signals in streamflow, obtained by varying the SAS shape parameter  $\alpha$  in groundwater, are shown in Figure 8. For the HOAL catchment,  $r$  values ranged from 0.54 to 0.60, indicating that, in contrast to the root-zone, changes in the groundwater SAS function had minimal impact on the fit

between simulated and observed  $\delta^2\text{H}$  signals (Fig. 8a). In the Wüstebach catchment,  $r$  values only slightly increased from 0.71 ( $\alpha = 0.1$ ) to 0.76 ( $\alpha = 1.0$ ) before decreasing slightly at  $\alpha = 5.0$  to 0.75. In both catchments, the correlations remained consistently strong across all  $\alpha$  values tested (Fig. 8a, b).

A stronger preference for young water ( $\alpha = 0.1$ ) led to approximately 25 % of streamflow being younger than 1000 days in the HOAL (Fig. 10a) and 35 % in the Wüstebach (Fig. 10b). In contrast, an older-water preference ( $\alpha = 5.0$ ) shifted the distribution and reduced the proportion of streamflow being younger than 1000 days around to 5% in the HOAL and to 12% in the Wüstebach. This shift, resulting from changing the SAS function parameter  $\alpha$  from 0.1 to 5.0, produced a variability of approximately 20 % in HOAL and 23 % in Wüstebach in the proportion of streamflow composed of water younger than 1000 days (Fig. 10a, b).

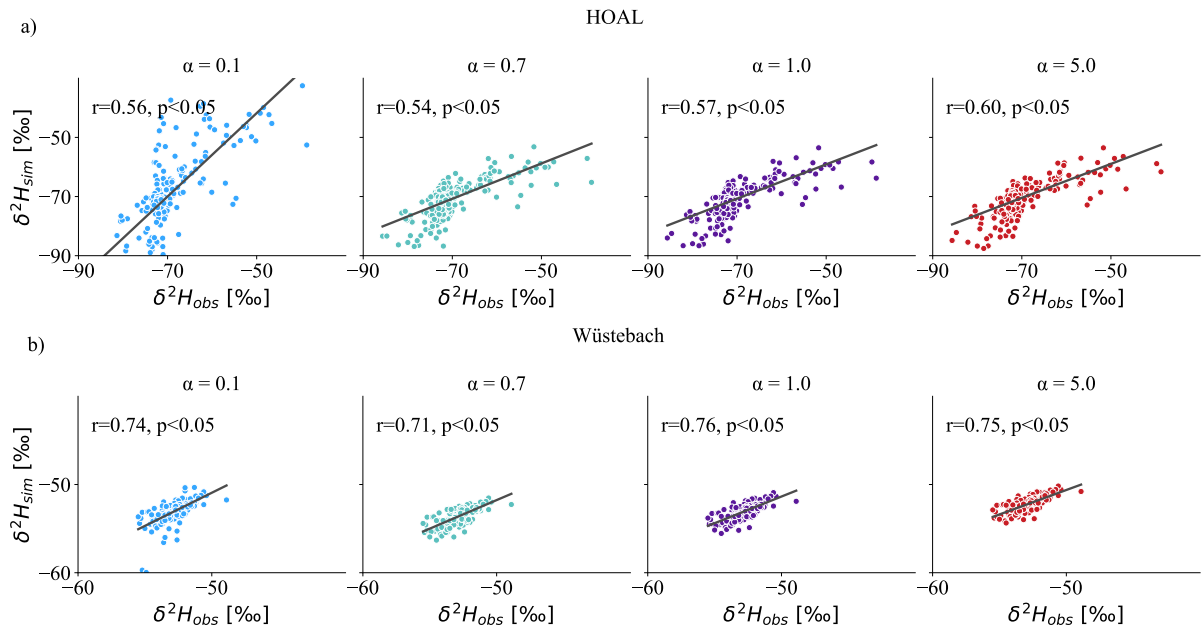


**Figure 8.** Spearman rank correlations between simulated (y-axis) and observed (x-axis)  $\delta^2\text{H}$  signals in streamflow based on varying the SAS shape parameter  $\alpha$  [-] in groundwater for (a) HOAL and (b) Wüstebach. The simulations ranged from very young water preference ( $\alpha = 0.1$ ) to old water preference ( $\alpha = 5$ ) for the groundwater, while for the root zone compartment, a calibrated value was used ( $\alpha_0 = 0.14$  for HOAL and 0.98 for Wüstebach).

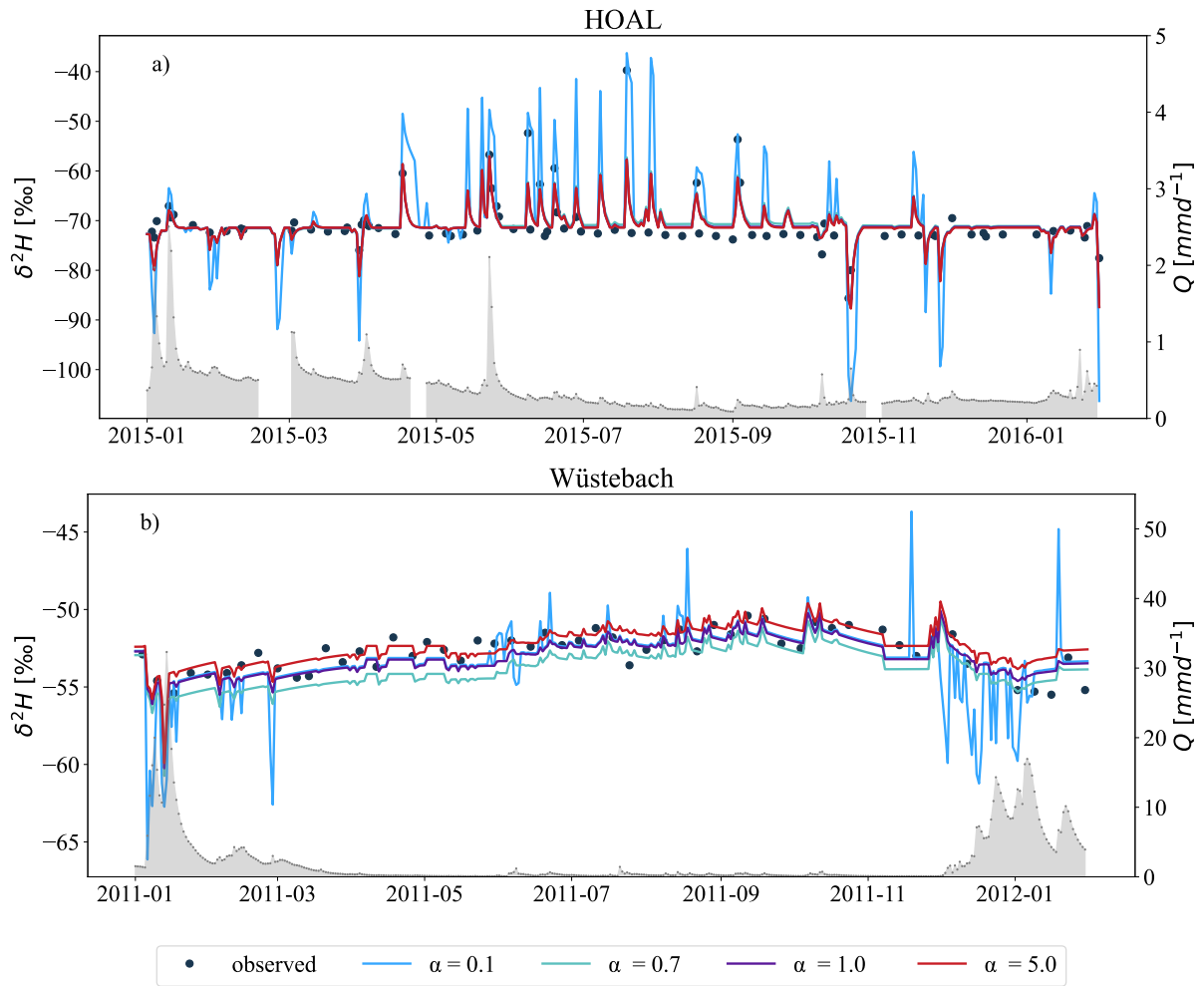


**Figure 9.** Simulation of  $\delta^2H$  in streamflow based on varying SAS shape parameter  $\alpha$  [-] in groundwater for (a) HOAL, [shown for 2015](#) and (b) Wüstebach, [shown for 2011](#). Simulations over the full tracking period are provided in Figure S 8. The simulations ranged from very young water preference ( $\alpha = 0.1$ ) to old water preference ( $\alpha = 5$ ) for the groundwater, while for the root zone compartment, a calibrated value was used ( $\alpha_0 = 0.14$ , for HOAL and 0.98 for Wüstebach). The simulated  $\delta^2H$  signals from the model are illustrated with blue, turquoise, purple, and red lines corresponding to  $\alpha$  values of 0.1, 0.7, 1.0, and 5.0, respectively. The grey-shaded area shows the measured streamflow ( $Q$ ,  $\text{mm d}^{-1}$ ) for both catchments.

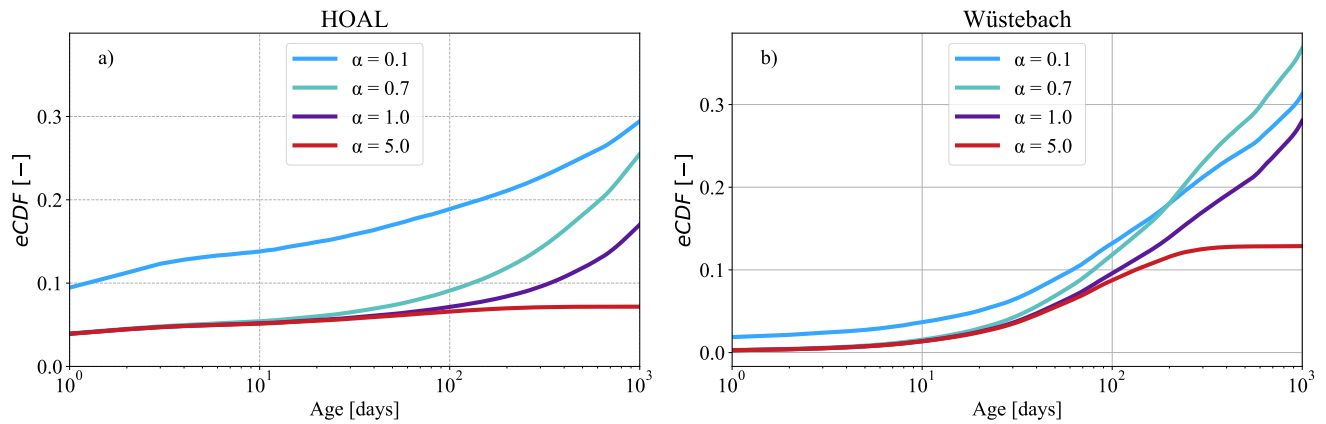


**Figure 10.** The mean of empirical cumulative distribution functions (eCDFs) of simulated transit times of daily discharge for the (a) HOAL and (b) Wüstebach catchments under varying SAS shape parameters ( $\alpha = 0.1, 0.7, 1.0, 5.0$ ) for groundwater. Lower  $\alpha$  values favour younger water, producing younger transit time distributions, while higher  $\alpha$  values shift the distribution toward older water. The mean of inferred TTD lines are illustrated with blue, turquoise, purple, and red lines corresponding to  $\alpha$  values of 0.1, 0.7, 1.0, and 5.0, respectively. (a–b) The simulations ranged from very young water preference ( $\alpha = 0.1$ ) to old water preference ( $\alpha = 5$ ) for the groundwater, while for the root zone compartment, a calibrated value was used ( $\alpha_0 = 0.14$ , for HOAL and 0.98 for Wüstebach).

### 3.6 Variation in the streamflow tracer signal and TTD estimations under different passive storage volumes and mixing assumptions

480 The results addressing the extent to which passive storage volume and associated mixing assumptions influence the representation of preferential groundwater flow, the estimated transit time distributions, and the interpretation of tracer signals at the catchment scale, are presented in Figures 11 and 12. Briefly, ~~and somewhat surprisingly,~~ the findings show that increasing the passive storage volume dampens the contribution of young water, shifts the overall transit time distribution towards older ages, and reduces variability in the  $\delta^2\text{H}$  signal variability in streamflow.

485 Simulations with varying  $S_{S,p}$  volumes and different mixing assumptions (Figs. 11, 12) resulted in distinct  $\delta^2\text{H}$  responses in streamflow. In both catchments, an active storage volume ~~rate~~-equivalent to approximately 1% of the passive storage volume was needed to attenuate the simulated tracer signal in line with observations. In the HOAL, a passive storage volume of  $S_{S,p} = 500$  mm (Fig. S 9a) was sufficient to achieve this, while in Wüstebach, a much larger volume of  $S_{S,p} = 5000$  mm was necessary (Fig. S 9 b). SAS shape parameters indicating a young-water preference ( $\alpha = 0.1$ ) resulted in variable  $\delta^2\text{H}$  signals in streamflow, whereas an older-water preference ( $\alpha = 5.0$ ) led to stronger dampening (Figs. 11, 12). Once the volume ~~rate ratio~~ between active and passive storage fell below 1%, further increases in  $S_{S,p}$  had little effect on model performance (Table 2). The ~~Nash–Sutcliffe Efficiency (NSE)~~ NSE remained relatively stable across different  $S_{S,p}$  values, with moderate improvements for  $\alpha = 0.7, 1.0, \text{ and } 5.0$ . In contrast, simulations with  $\alpha = 0.1$  yielded negative NSE values (Table 2). The highest  $\text{NSE}_{\delta^2\text{H}}$  values—approximately 0.55—were achieved with  $\alpha = 1.0$  and  $\alpha = 5.0$  for the HOAL catchment. The results

495 in the Wüstebach catchment exhibited a wider range of NSE values, from  $-11.25$  to  $0.22$ , as  $S_{S,p}$  increased, suggesting that model performance was more sensitive to the size of the passive storage volume than to the shape factor  $\alpha$ .

In both catchments, increased passive storage volumes influenced the old tail of transit times ( $100 < T < 1000$  days). Increasing  $S_{S,p}$  increased the probability of older water contributing to streamflow (Figs. 11, 12) and reduced the fraction of streamflow younger than 1000 days substantially. The range of differences in the fraction of streamflow younger than 1000 days varied across different mixing assumptions, yet remained consistent overall. In the HOAL catchment (Fig. 11 a-c), under the uniform sampling assumption, the fraction of streamflow younger than 1000 days decreased from 50 % to 5 % as  $S_{S,p}$  increased from 500 mm to 5000 mm. Given that model performance remained similar across these scenarios (Table 2), this implies a variability of approximately 45 % in TTD estimation attributable to ~~passive storage volume alone~~uncertainties in passive storage volumes. In the Wüstebach catchment (Fig. 12 a-c), the corresponding fraction declined from 80 % to 45 %.

505 None of the simulations with  $S_{S,p}$  less than 5000 mm adequately reproduced the observed  $\delta^2\text{H}$  signal, suggesting that at least 50 % of stream water in Wüstebach is older than 1000 days.

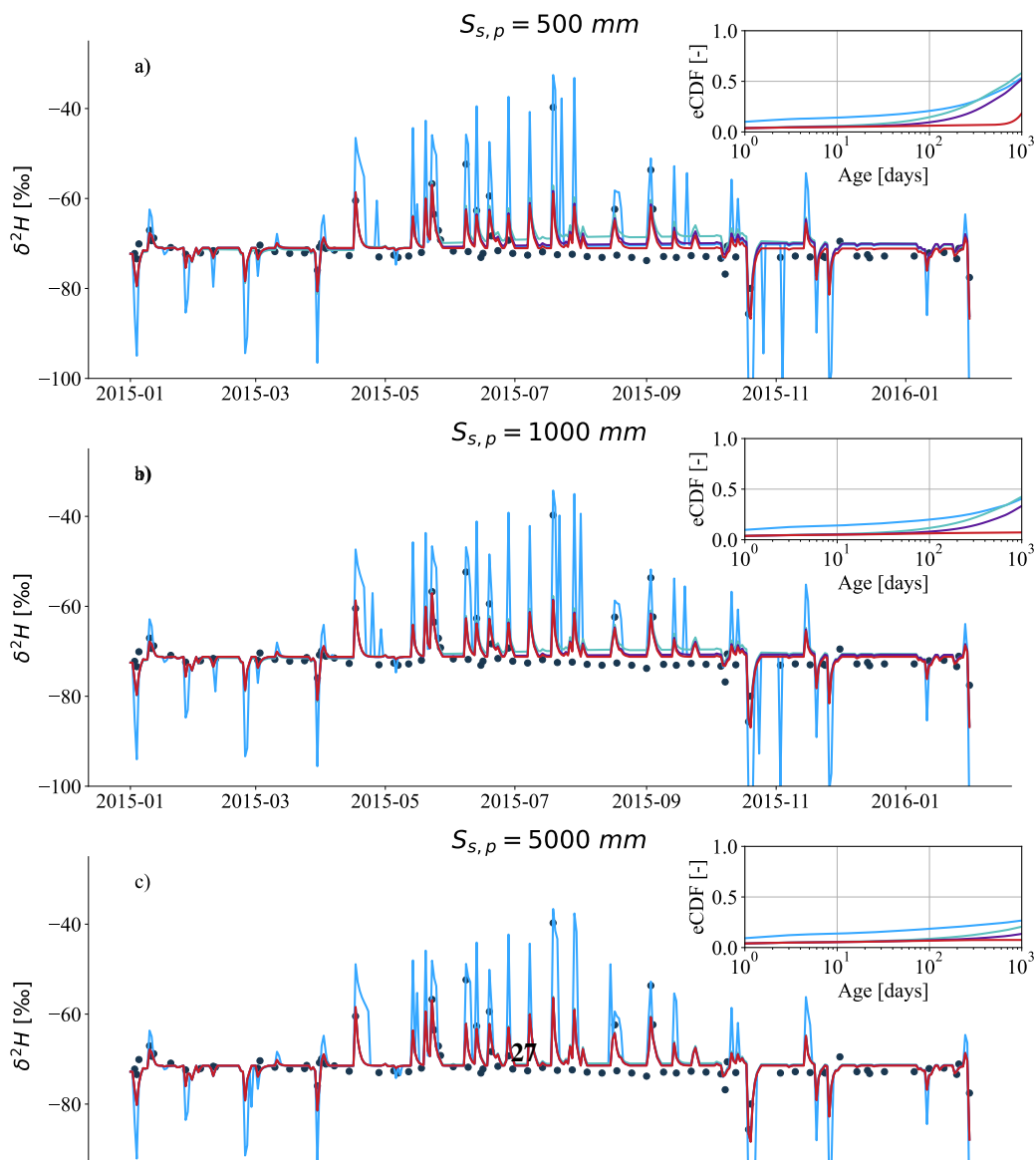
~~Simulated  $\delta^2\text{H}$  signals in streamflow ( $Q$ ;  $\text{mm d}^{-1}$ ) for the HOAL catchment in the year 2015, based on varying passive groundwater storage volumes ( $S_{S,p} = 500$  mm, 1000 mm, and 5000 mm) and different mixing assumptions defined by SAS function shape parameters ( $\alpha = 0.1, 0.7, 1.0, \text{ and } 5.0$ ). (a-c) each plot shows results for one  $S_{S,p}$  value, with black dots indicating observed grab samples of streamflow  $\delta^2\text{H}$ , and coloured lines representing simulated  $\delta^2\text{H}$  under the different  $\alpha$  values. The inset in each plot shows the mean empirical cumulative distribution functions (CDF) of simulated daily streamflow transit times during the tracking period (2015–2019); line colours correspond to  $\alpha$  values: blue for 0.1, turquoise for 0.7, purple for 1.0, and red for 5.0. Simulations over the full tracking period (2015–2019) are provided in the Supplement S-10.~~

510 ~~Simulated  $\delta^2\text{H}$  signals in streamflow ( $Q$ ;  $\text{mm d}^{-1}$ ) for the Wüstebach catchment in the year 2011, based on varying passive groundwater storage volumes ( $S_{S,p} = 500$  mm, 1000 mm, and 5000 mm) and different mixing assumptions defined by SAS function shape parameters ( $\alpha = 0.1, 0.7, 1.0, \text{ and } 5.0$ ). (a-c) each plot shows results for one  $S_{S,p}$  value, with black dots indicating observed grab samples of streamflow  $\delta^2\text{H}$ , and coloured lines representing simulated  $\delta^2\text{H}$  under the different  $\alpha$  values. The inset in each plot shows the mean empirical cumulative distribution functions (eCDFs) of simulated daily streamflow transit times during the tracking period. Line colours correspond to  $\alpha$  values: blue for 0.1, turquoise for 0.7, purple for 1.0, and red for 5.0. Simulations over the full tracking period (2011–2013) are provided in the Supplement S-11.~~

520

**Table 2.** Performance metrics for simulated  $\delta^2\text{H}$  values in the HOAL (from 2015 to 2019) and Wüstebach (from 2011 to 2013) catchments under varying passive groundwater storage volumes ( $S_{s,p}$ ) and groundwater SAS function shape parameters ( $\alpha$ ). For each  $S_{s,p}$  volume (500 mm, 1000 mm, and 5000 mm), simulations were run with  $\alpha$  values representing a range from very young-water preference ( $\alpha = 0.1$ ) to old-water preference ( $\alpha = 5.0$ ). The root zone SAS function was fixed at its calibrated value for each catchment ( $\alpha_0 = 0.14$  for HOAL and 0.98 for Wüstebach). Performance was evaluated using the Nash–Sutcliffe Efficiency ( $\text{NSE}_{\delta^2\text{H}}$ ) and Mean Absolute Error ( $\text{MAE}_{\delta^2\text{H}}$ ) between observed and simulated streamflow  $\delta^2\text{H}$  signals.

Catchment	Metric	$S_{s,p} = 500 \text{ mm}$				$S_{s,p} = 1000 \text{ mm}$				$S_{s,p} = 5000 \text{ mm}$			
		$\alpha = 0.1$	0.7	1.0	5.0	0.1	0.7	1.0	5.0	0.1	0.7	1.0	5.0
HOAL	$\text{NSE}_{\delta^2\text{H}}$	-1.20	0.49	0.55	0.55	-1.02	0.53	0.55	0.56	-0.68	0.55	0.56	0.56
	$\text{MAE}_{\delta^2\text{H}}$	5.34	2.92	2.60	2.67	5.00	2.70	2.51	2.50	4.55	2.53	2.49	2.49
Wüstebach	$\text{NSE}_{\delta^2\text{H}}$	-11.25	-12.52	-13.34	-12.17	-5.77	-7.58	-6.88	-8.08	0.14	-0.44	0.31	0.22
	$\text{MAE}_{\delta^2\text{H}}$	3.70	3.74	4.04	3.64	2.77	3.05	3.04	2.84	0.77	1.16	0.76	0.81



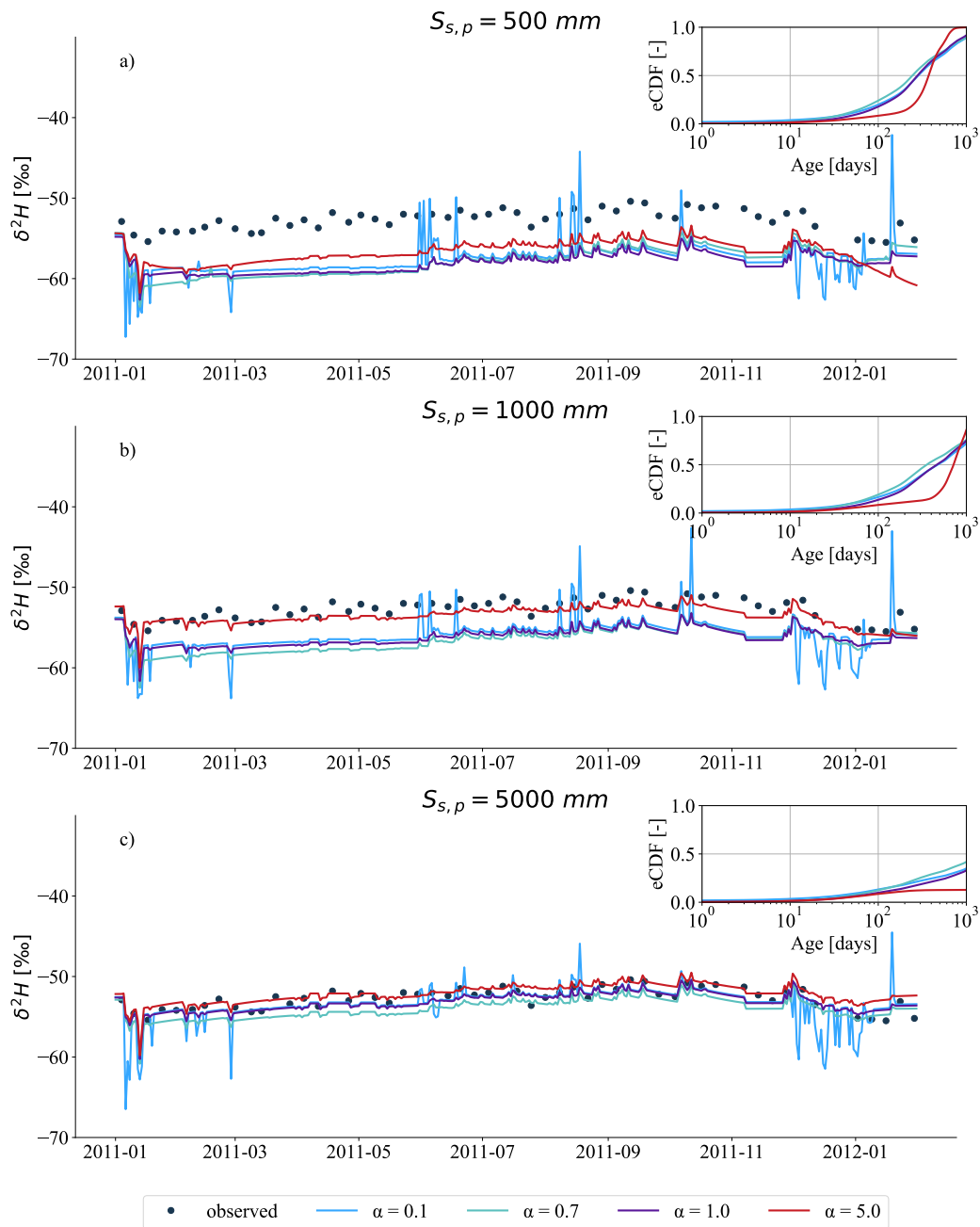


**Figure 12.** Simulated  $\delta^2\text{H}$  signals in streamflow ( $Q$ ;  $\text{mm d}^{-1}$ ) for the Wüstebach catchment in the year 2011, based on varying passive groundwater storage volumes ( $S_{S,p} = 500 \text{ mm}$ ,  $1000 \text{ mm}$ , and  $5000 \text{ mm}$ ) and different mixing assumptions defined by SAS function shape parameters ( $\alpha = 0.1, 0.7, 1.0$ , and  $5.0$ ). (a-c) each plot shows results for one  $S_{S,p}$  value, with black dots indicating observed grab samples of streamflow  $\delta^2\text{H}$ , and coloured lines representing simulated  $\delta^2\text{H}$  under the different  $\alpha$  values. The inset in each plot shows the mean empirical cumulative distribution functions (eCDFs) of simulated daily streamflow transit times during the tracking period. Line colours correspond to  $\alpha$  values: blue for 0.1, turquoise for 0.7, purple for 1.0, and red for 5.0. Simulations over the full tracking period (2011–2013) are provided in the Supplement S 11.

## 4 Discussion

### 4.1 Comparison of catchment transit times

The inferred transit times in HOAL (13 % of streamwater younger than 1000 days) and Wüstebach (27 % of streamwater younger than 1000 days) indicated that, in both catchments, the majority of water contributing to streamflow was relatively old—consistent with findings from many other catchments (Kirchner et al., 2023; Floriancic et al., 2024; Wang et al., 2025). During wet periods, the fraction of water  $T < 1000$  days was 15 % in HOAL and 33 % in Wüstebach; in dry periods, these values dropped to 10 % and 22 %, respectively. This variation indicated a greater release of younger water under wetter conditions, consistent with other studies (Klaus et al., 2013; Angermann et al., 2017; Loritz et al., 2017). In Wüstebach, relatively high soil ~~moisture-wetness~~ and high monthly mean young-water fractions ranging from 5 % to 15 % (Figs. 5e, f) pointed to wet-soil promotion of preferential flow which has been observed previously (Wiekenkamp et al., 2016; Stockinger et al., 2014; Hrachowitz et al., 2021; Hövel et al., 2024). By contrast, HOAL's younger-water release did not depend on soil ~~moisture-wetness~~ only; instead, rapid flow pathways (e.g. infiltration-excess overland flow, macropores, tile drains) as known for this catchment (Exner-Kittridge et al., 2016; Pavlin et al., 2021; Vreugdenhil et al., 2022) allowed water to bypass much of the soil matrix and reach the stream quickly, even under dry conditions, which ~~is consistent with~~ was discussed in previous findings (Türk et al., 2024; Széles et al., 2020). ~~Given the~~ The consistency of our results with prior tracer-based ~~modelling-modeling~~ and SAS applications in both HOAL (Széles et al., 2020; Türk et al., 2024) and Wüstebach (Stockinger et al., 2019; Hrachowitz et al., 2021) ~~provides confidence in~~ the applied model configurations ~~were considered reasonable and reliable~~. ~~However, we acknowledge that such consistency alone cannot exclude the possibility of shared assumptions. Therefore, we use these results as supporting evidence that the model setups are reasonable~~ for testing the research hypotheses ~~in this study, while recognizing the need for further validation with complementary data and approaches.~~

### 4.2 Do stream water tracer data have sufficient ~~information content variability~~ to identify preferential flow in the unsaturated root zone and in groundwater using different SAS functions?

~~The stepwise analysis presented in Figure 6 and Table 1 indicated~~ Positive correlations between modeled and observed streamflow tracer signals (Fig. 6a,b), together with high model-efficiency metrics at lower  $\alpha_0$  values (indicating a preference for younger water; Table 1), show that streamflow tracer data were sufficiently sensitive to ~~identify the SAS parameterization of~~ preferential flow in the ~~shallow~~ unsaturated zone for both the HOAL and ~~the~~ Wüstebach catchments. This suggests rapid transport of precipitation through preferential flow pathways in both catchments, consistent with previous findings (Wiekenkamp et al., 2016). Specifically, changing the root-zone SAS shape parameter  $\alpha_0$  produced clear differences in simulated streamflow  $\delta^2\text{H}$  signals (Fig. 6), demonstrating ~~tracer data sensitivity to young water release via shallow subsurface pathways (Stockinger et al., 2016; Benettin et al., 2016).~~ Positive correlations and model efficiency metrics at lower  $\alpha_0$  values (indicating a preference for younger water, Table 1) supported this interpretation, indicating rapid transport of precipitation through preferential routes in both catchments, which is consistent with previous findings (Wiekenkamp et al., 2016; Stockinger et al., 2014; Széles et al., 2020) tracer data sensitivity to young water release. The results, quantitatively demonstrated through the SAS-based modeling framework, show that

streamflow isotope data can reflect the activation of preferential flow in the unsaturated zone. While previous studies have identified such processes through field observations (Vreugdenhil et al., 2022; Pavlin et al., 2021; Wiekenkamp et al., 2016), our results demonstrate that they can also be captured and interpreted using catchment-scale tracer modeling.

Nevertheless, there were differences in the the two catchments exhibited distinct processes controlling preferential flow in the unsaturated root zone. The calibrated lower boundary of the SAS function shape parameter,  $\alpha_0$ , differed between the two catchments markedly ( $\alpha_0 = 0.14$  for HOAL and  $\alpha_0 = 0.98$  for Wüstebach), suggesting distinct internal catchment characteristics that control the Wüstebach), reflecting contrasting storage–discharge relationship in the unsaturated root zone relationships and preferential flow activation. For HOAL, an mechanisms in the unsaturated zone. In HOAL, the low  $\alpha_0$  of 0.14 value indicated rapid, direct overland flow processes water transmission through preferential flow paths driven by intense rainfall, consistent with previous hydrometric analyses and field observations (Pavlin et al., 2021; Vreugdenhil et al., 2022). This rapid flow, which allow young water to reach the stream with limited mixing. This was further facilitated by soil crust formation the formation of soil crusts and cracking of the clay-rich topsoil during the dry summer months, creating direct preferential pathways that quickly transport water accelerate water transmission through the catchment (Exner-Kittridge et al., 2016). In contrast, the forest cover in Wüstebach promotes higher infiltration rates, enhancing subsurface mixing (Wiekenkamp et al., 2016) compared to the HOAL catchment. Despite these differences, findings from both catchments align higher  $\alpha_0$  value in Wüstebach ( $\alpha_0 = 0.98$ ) indicated that under wetter antecedent conditions, established preferential flow pathways promoted greater subsurface mixing, leading to relatively older water contributions. This likely reflects the influence of forest cover in Wüstebach, where enhanced infiltration promotes deeper and more uniform mixing (Wiekenkamp et al., 2016) than in HOAL. Despite contrasting site characteristics, both catchments showed responses consistent with previous studies that have generally documented the importance documented the role of macropores and preferential flow pathways in the unsaturated zone, highlighting that where water frequently bypasses matrix storage and exchange processes (Zehe et al., 2006; Angermann et al., 2017; Sprenger et al., 2016; Klaus et al., 2013; Loritz et al., 2017), as it was reflected in the SAS formulation through model calibration (Hrachowitz et al., 2013; van der Velde et al., 2015). These results underline the need to calibrate, rather than assume, root zone SAS parameters when estimating transit times.

The Spearman rank correlations ( $r$ ) between observed and simulated  $\delta^2\text{H}$  were lower in HOAL compared to Wüstebach, which can be attributed in part to differences in temporal resolution and the variability of isotope sampling. In HOAL, streamflow  $\delta^2\text{H}$  was sampled on an event basis, with values ranging from  $-26.2\text{‰}$  to  $-108.0\text{‰}$  (Fig. 1b). In contrast, the Wüstebach catchment weekly to biweekly sampling scheme, yielding streamflow  $\delta^2\text{H}$  values between  $-45.6\text{‰}$  and  $-57.1\text{‰}$  (Fig. 1b). Although model performance metrics such as NSE or correlation coefficients quantify the agreement between simulated and observed isotope time series, they can result in seemingly good fits in the presence of sparse or irregular data sampling (Beven, 2006) and influence TT estimation (Stockinger et al., 2016).

Streamflow On the other hand, streamflow tracer  $\delta^2\text{H}$  showed limited sensitivity to variations in groundwater SAS function shape parameters (Fig. 8, Table 1). Our conceptual tracer-based model simulations indicated minimal differences in simulated  $\delta^2\text{H}$  signals across various groundwater SAS shapes, including accounting for preferential flow in groundwater. In the HOAL catchment, the Spearman rank correlation ( $r$ ) varied slightly (0.54–0.60) among different groundwater  $\alpha$  values. Similarly,

590 correlations remained relatively stable in the Wüstebach catchment, peaking at  $r = 0.76$  for  $\alpha = 1.0$ , but showing little variation overall. These results suggest that  $\delta^2\text{H}$  tracer, suggesting that isotope data alone may not carry sufficient information to clearly distinguish provide sufficient variability to resolve preferential groundwater flow dynamics at the catchment scale.

This is supported by the small variation in correlation strength across different  $\alpha$  settings, with  $r = 0.54\text{--}0.60$  in the HOAL catchment and  $r = 0.71\text{--}0.76$  in Wüstebach. We attributed this insensitivity to the substantial limited variability to the large passive groundwater storage volumes (3117 formulated within the model (approximately 500 mm in HOAL and 9976 mm in Wüstebach)–5000 mm in W"ustebach;), which act to buffer hydrological variability and result in comparable model performance once the storage threshold is exceeded Table 2). It should be noted that these values represent modeled estimates rather than their actual physical magnitude and therefore reflect a parameterization that buffers the effect of preferential groundwater flow on  $\delta^2\text{H}$  simulations. In our and many other catchment scale modelling approaches (Benettin et al., 2015a; Hrachowitz et al., 2013; Wang et al., 2023, 2025), groundwater ( $Q_S$ ) age selection is formulated based on age samples from the total groundwater storage ( $S_{S,\text{tot}}$ ), combining contributions from both active ( $S_{S,a}$ ) and passive ( $S_{S,p}$ ) compartments (Zuber, 1986; Hrachowitz et al., 2015). Thus, the age-ranked groundwater storage ( $S_{T,S,\text{tot}}$ ) inherently reflected a mixture of these storage volumes. Substantial passive storage characterised by long residence times strongly buffers the isotopic signals in streamflow (Birkel et al., 2011a), effectively masking distinct signatures of preferential groundwater flow, as is the case in our catchments too. Although our Although the model explicitly allowed preferential recharge of younger groundwater (e.g.,  $R_{fs}$ , Fig. 2), subsequent mixing within the large passive groundwater storage dampened  $\delta^2\text{H}$  in streamflow the passive storage, characterized by long residence times, buffers the isotopic signals in streamflow (Birkel et al., 2011a), thereby masking the distinct signatures of preferential groundwater flow. Consequently, varying the groundwater SAS shape had negligible limited effects on simulated streamflow  $\delta^2\text{H}$  dynamics within the parameter ranges tested here.

The sensitivity of tracer signals to passive storage volumes further underscored the uncertainty introduced by the conceptual storage parameters. In both catchments, the isotope signals were substantially dampened when the volume ratio between active and passive storages ( $S_{S,a}/S_{S,p}$ ) fell below 1%. Even maximal mixing between compartments thus appeared sufficient to markedly reduce isotopic variations, particularly when large passive volumes buffered hydrological responses. Nevertheless, the absolute storage volume required to achieve the observed isotope damping differed notably between the two catchments. In HOAL, model performance remained stable across a wide range of passive storage volumes above 500 mm (e.g.,  $\text{NSE}_{\delta^2\text{H}} \approx 0.55$  for both  $S_{S,p} = 500$  mm and  $S_{S,p} = 6117$  mm), suggesting high uncertainty in estimating the upper bound of passive storage. In contrast, model performance in Wüstebach improved significantly with larger passive storage volumes (Table 2), consistent with previous observations by Hrachowitz et al. (2021), who argued for substantial passive storage ( $\sim 8000$  mm) to replicate observed isotope damping patterns. Spearman rank correlations ( $r$ ) between observed and simulated  $\delta^2\text{H}$  were lower in HOAL compared to Wüstebach, which can be attributed to differences in temporal resolution and the variability of isotope sampling (Fig. 1a, b). Although model performance metrics, such as NSE or correlation coefficients, quantify the agreement between simulated and observed isotope time series, they can result in seemingly good fits in the presence of sparse or irregular data sampling (Beven, 2006). In such cases, deceptively high NSE values may still occur even when key groundwater age-selection

parameters (e.g., preference for young vs. old water) remain poorly constrained, thereby affecting transit time estimations (Stockinger et al., 2016).

625 An alternative explanation, however, must also be considered: it is possible that such preferential groundwater flow processes are simply absent or negligible in the HOAL and Wüstebach catchments. The current data and model structure are insufficient to conclusively rule out either possibility. Ultimately, distinguishing between limitations in model sensitivity and the actual absence of preferential flow processes requires additional, spatially distributed tracer data and complementary hydrometric observations.

630 **4.3 Does accounting for preferential groundwater flow (and associated through a SAS functions) function affect catchment-scale transit time distributions?**

SAS function shape changes in groundwater only marginally affected model performance. Different groundwater mixing assumptions yielded similar isotope model fits (Table 2), with the exception of the except for the case with a strong young-water preference ( $\alpha = 0.1$ ) in the HOAL catchment. This suggests that differences in mixing assumptions had limited influence on model fit. However, the associated corresponding transit time distributions (TTDs) were substantially different, and thus, the estimation of TT is uncertain differed substantially, revealing that TTD estimates remain highly uncertain with the available isotope data. Consistent with previous findings studies (van der Velde et al., 2012; Borriero et al., 2023), our results highlighted that TTD estimates are highly findings emphasize that TTDs are particularly sensitive to how groundwater SAS functions are conceptualised and parameterised conceptualized and parameterized within the model.

640 Specifically, the empirical cumulative distribution functions (eCDFs) of simulated TTDs (Fig. 10) revealed notably different ranges: assuming a strong young-water preference ( $\alpha = 0.1$ ) resulted in the fraction yielded fractions of streamflow younger than 1000 days to of approximately 25 % in HOAL and 35 % in Wüstebach Wüstebach, whereas an older-water preference ( $\alpha = 5.0$ ) reduced these fractions to around 5 % and 12 %, respectively (Fig. 10). This variability in transit time estimations for  $T < 1000$  estimates for  $T < 1000$  days—roughly about 20 % for in HOAL and 23 % for Wüstebach in Wüstebach—underscores a critical limitation in modelling highlights a key limitation: groundwater transit times derived from SAS functions remain highly uncertain, even when overall model performance is similar.

Given these uncertainties arising from groundwater SAS function shapes alone, it is also crucial to assess how passive groundwater storage volumes, through their mixing with active groundwater storage, further modulate transit time estimates. Our results indicated that

650 **4.4 How do groundwater mixing assumptions and passive storage volumes influence tracer simulation and transit time estimation at the catchment scale?**

In both HOAL and Wüstebach catchments, isotope signals were attenuated when the ratio between active and passive storage ( $S_{S,a}/S_{S,p}$ ) fell below 1 % (Figs. 11, 12). This indicates that the passive groundwater storage was much larger—typically about one order of magnitude greater than the active storage, as also reported by Birkel et al. (2011a)—and acted as an effective buffer that dampened isotope variability in streamflow and constrained the model's ability to resolve young-water dynamics.

In HOAL, model performance remained comparable across a wide range of passive storage volumes above 500 mm (e.g.,  $NSE_{\delta^2H} \approx 0.55$ ), suggesting considerable uncertainty in the upper bound of passive storage for any volume exceeding this threshold. In contrast, model performance in Wüstebach improved with increasing passive storage (Table 2), consistent with previous findings by Hrachowitz et al. (2021), who proposed substantial groundwater storage ( $\sim 8000$  mm) to reproduce observed isotope damping. Nevertheless, the stepwise analysis showed that similar performance ( $NSE_{\delta^2H} = 0.31$ ) could also be achieved with  $S_{S,p} = 5000$  mm and uniform mixing, reinforcing the large uncertainty in constraining the upper range of passive storage volumes substantially influenced the longer tails of the inferred TTDs, highlighting their importance in catchment transit time estimation in catchment-scale models. Given the uncertainties in passive storage parameters, it is crucial to assess how passive groundwater storage, combined with active storage, influences estimated transit time distributions (TTDs). In both catchments, we observed a clear negative correlation emerged between passive storage volume and the fraction of streamflow younger than 1000 days (Figs. 11, 12). For instance, under a uniform sampling assumption, the fraction of young water decreased markedly—Under uniform sampling assumptions, the young-water fraction decreased from approximately 45 % to 10 % in HOAL and from about 85 % to 25 % in Wüstebach—as passive storage in Wüstebach as  $S_{S,p}$  increased from 500 mm to 5000 mm (Fig. 12). Since the SAS function was formulated based on age-ranked total groundwater storage ( $S_{S,tot} = S_{S,a} + S_{S,p}$ ), larger passive storage volumes increased the probability likelihood of older water contributions to streamflow, thereby extending the tails of the TTDs ( $100 < T < 1000$  days).

#### 4.5 Implications and limitations

The methodological framework applied here, including the stepwise analysis of SAS functions and the incorporation of multiple passive storage volumes, offered a systematic approach that could be adapted to other regions and TTD studies. Nonetheless, the uncertainty resulting from the specific model setup and parameter choices used in this study cannot be directly generalised across diverse catchments or hydrological conditions. Addressing these limitations, e.g. for example, by improving the monitoring frequency of (isotope) hydrological data, integrating additional tracers such as tritium ( $^3H$ ), and refining model representations of subsurface processes, will be essential for reducing uncertainty and enhancing the reliability of SAS-based modelling.

While our study focused on a lumped catchment-scale framework, the results highlighted the need to advance toward more distributed models that can more directly link spatial heterogeneity in soils, slopes, and storage to preferential flow dynamics and advance process understanding. At the catchment scale, isotope-based modeling proved useful in capturing preferential flow in the unsaturated zone, but was limited in doing so in groundwater due to the damping of the seasonal signal of water stable isotopes by large passive storage volumes assumed in the models. This suggests that in catchments with similar damped water stable isotope signals, groundwater age selection will be difficult to constrain.

While the SAS formulation identifies the statistical signatures of preferential flow through tracer-based modeling, it does not explicitly resolve the physical mechanisms that induce preferential flow. Therefore, isotope data alone, when used within a catchment-scale lumped model framework, may be insufficient to distinguish between a true absence of preferential flow and a limited model sensitivity to detect it. In the HOAL catchment, Exner-Kittridge et al. (2016) showed that alternating

690 contributions from shallow and deep aquifers throughout the year were the main cause of the seasonal variability in nitrate concentrations in streamflow. These alternating contributions, together with extensive tile drainage and heterogeneous clay-rich soils, create rapid and spatially variable flow pathways (Exner-Kittridge et al., 2016; Pavlin et al., 2021). Such features, combined with overland flow of the HOAL catchment (Blöschl et al., 2016), may favor the activation of preferential flow. For the Wüstebach catchment, field studies indicated that soil and groundwater dynamics are coupled. Bogena et al. (2015) and Graf et al. (2014)  
695 showed that soil water variability decreases with depth due to lower porosity and root water uptake in shallow depth, while groundwater fluctuations closely follow soil moisture dynamics (Bogena et al., 2015), reflecting high infiltration and storage capacity in forest soils. This behaviour contrasts with the results obtained in the HOAL catchment, suggesting a more uniform subsurface mixing in Wüstebach. Although these processes remain beyond the explicit resolution of top-down, isotope-based transport models, the SAS framework enables delineation of the hydrological conditions under which preferential flow effects  
700 become detectable. Future research should combine stable isotopes with complementary tracers (e.g., tritium, chloride, or major ions) and higher-frequency sampling to enhance the diagnostic power of tracer-aided models. Furthermore, linking SAS function shapes to measurable catchment attributes could enable *a priori* parameterization, thereby reducing dependence on calibration. At the lysimeter pedon scale, Asadollahi et al. (2020) showed that SAS functions can approximate the analytical solution of the advection–dispersion equation; however, extending such mechanistic relationships to the catchment scale  
705 remains challenging within lumped “bucket” model frameworks. Addressing these challenges represents a key step toward integrating empirical SAS modeling with a process-based understanding of preferential flow and subsurface mixing.

## 5 Conclusion

In this study, we evaluated whether stream water isotope data ~~provide adequate information to identify and quantify~~ contain sufficient variability to simulate preferential flow in the unsaturated zone and in groundwater using various StorAge Selection (SAS) function ~~shapes at the catchment scale~~ parametrizations within a catchment-scale transport model. We further analysed the implications of explicitly representing preferential ~~root zone~~ root-zone and groundwater flow ~~and, as well as~~ passive storage volumes, on the estimation of transit time distributions (TTDs). ~~Our findings underscore~~ The findings indicated that streamflow tracer data were sufficiently sensitive to the SAS parameterization of preferential flow in the shallow unsaturated zone. However, the results also revealed critical limitations in using isotope tracer data alone to constrain groundwater transit  
715 times, ~~emphasising the due to the strong~~ influence of passive groundwater storage on ~~uncertainty in catchment-scale models.~~ model uncertainty at the catchment scale.

The main findings of our study are:

- Streamflow isotope ( $\delta^2\text{H}$ ) data were sensitive enough to characterise preferential flow processes in the unsaturated root zone, confirming that such processes significantly shape catchment isotope signatures and transit time distributions at  
720 short timescales (up to 300 days). ~~This highlighted the need to calibrate, rather than assume, root zone SAS parameters when estimating transit times.~~

- Streamflow isotope data alone were insufficient to differentiate among groundwater SAS function shapes for the two tested catchments. Large passive groundwater storage volumes significantly dampened isotopic variations, making it impossible to clearly identify preferential flow in groundwater.
  - 725 – The variability in groundwater TTD estimates arising from varying SAS function shapes for groundwater was considerable ( 20 % for HOAL and 23 % for Wüstebach), highlighting that TTD estimates are highly sensitive to how SAS functions are conceptualised and parameterised within the model.
  - ~~Passive groundwater storage volumes strongly controlled the~~ The size of the passive groundwater storage exerts a dominant control on catchment transit time ~~distributions, particularly affecting estimates, particularly influencing~~ the longer tails ( $T > 100$  days) ~~.Increasing passive storage reduced the fraction of younger streamflow ( $T < 1000$  days), of~~ the distributions, thereby introducing uncertainties into solute and contaminant transport predictions.
- 730

These findings carry implications beyond water transit times, also affecting the transport timescales of solutes and contaminants within catchments. Larger passive storage volumes imply prolonged retention times, potentially delaying pollutant transport and release. Consequently, uncertainty in estimating passive storage volumes directly translates into uncertainty regarding contaminant transport predictions, with critical implications for assessing water-quality risks. Additional or complementary datasets—such as direct groundwater measurements or higher-frequency tracer sampling—would be required to reliably characterise preferential groundwater flow using conceptual catchment-scale models. Improved characterisation of passive storage volumes—potentially via complementary observations (e.g., groundwater-level monitoring or high-frequency isotope sampling)—is essential to reduce uncertainties and enhance reliability in transit time and solute transport modelling at the catchment scale.

735

740

*Code and data availability.* A Python script that performs the calculations described in this paper will be deposited in an open-access Github archive repository, and the link will be supplied with the final published paper. The code repository for the *Tracer Transport Model* is available on GitHub at: [https://github.com/haticeturk/Tracer\\_Transport\\_Model.git](https://github.com/haticeturk/Tracer_Transport_Model.git). Model outputs, including state variables, fluxes, hydrological signatures, parameter sets, and performance metrics underlying this study, are available online in the FAIR-compliant Zenodo repository.

745 The meteorological and hydrological data from the Wüstebach TERENO site used in this study are openly accessible through the *Terrestrial Environmental Observatories (TERENO)* of the *Helmholtz Association of German Research Centers (HGF)*, Germany, via the TEODOOR data portal (<http://teodoor.icg.kfa-juelich.de/>). The stable water isotope dataset for the Wüstebach catchment is publicly available through a digital object identifier (DOI) at: <https://doi.org/10.34731/y6tj-3t38> (Bogena et al., 2021). The data for the HOAL catchment can be available from the Austrian Federal Agency for Water Management upon request.

750 *Author contributions.* HT performed the analysis presented here and drafted the paper. All authors discussed the design, contributed to the overall concept, and participated in the discussion and writing of the manuscript.

*Competing interests.* Some authors are members of the editorial board of the HESS journal.

*Acknowledgements.* We acknowledge the *Terrestrial Environmental Observatories (TERENO)* of the *Helmholtz Association of German Research Center (HGF)*, Germany, for providing access to the Wüstabach catchment data. We thank the Austrian Federal Agency for Water Management for providing the data the HOAL catchment that we used in our analysis. This research was funded by the *Austrian Science fully*  
755 *Fund by (FWF – Österreichischer Wissenschaftsfonds)* [Grant No. 10.55776/P34666]. For open access purposes, the author has applied a CC BY public copyright license to any ~~author-accepted~~author-accepted manuscript version arising from this submission. The work of Hatice ~~Türk~~Türk was supported by the Doctoral School "Human River Systems in the 21st Century (HR21)" of the BOKU University, Vienna.

## References

- 760 Ala-Aho, P., Tetzlaff, D., McNamara, J. P., Laudon, H., and Soulsby, C.: Using isotopes to constrain water flux and age estimates in snow-influenced catchments using the STARR (Spatially distributed Tracer-Aided Rainfall–Runoff) model, *Hydrology and Earth System Sciences*, 21, 5089–5110, 2017.
- Angermann, L., Jackisch, C., Allroggen, N., Sprenger, M., Zehe, E., Tronicke, J., Weiler, M., and Blume, T.: Form and function in hillslope hydrology: characterization of subsurface flow based on response observations, *Hydrology and Earth System Sciences*, 21, 3727–3748, 765 2017.
- Asadollahi, M., Stumpp, C., Rinaldo, A., and Benettin, P.: Transport and water age dynamics in soils: A comparative study of spatially integrated and spatially explicit models, *Water Resources Research*, 56, no–no, 2020.
- Benettin, P. and Bertuzzo, E.: tran-SAS v1.0: a numerical model to compute catchment-scale hydrologic transport using StorAge Selection functions, *Geoscientific Model Development*, 11, 1627–1639, 2018.
- 770 Benettin, P., Kirchner, J., Rinaldo, A., and Botter, G.: Modeling chloride transport using travel time distributions at Plynlimon, Wales, *Water Resources Research*, 51, 3259–3276, <https://doi.org/10.1002/2014WR016600>, 2015a.
- Benettin, P., Rinaldo, A., and Botter, G.: Tracking residence times in hydrological systems: Forward and backward formulations, *Hydrological Processes*, 29, 5203–5213, <https://doi.org/10.1002/hyp.10513>, 2015b.
- Benettin, P., Bailey, S., Rinaldo, A., Likens, G., McGuire, K., and Botter, G.: Young runoff fractions control streamwater age and solute 775 concentration dynamics, *Hydrological Processes*, 31, 2982–2986, <https://doi.org/10.1002/hyp.11243>, 2017.
- Berkowitz, B. and Zehe, E.: Surface water and groundwater: unifying conceptualization and quantification of the two “water worlds”, *Hydrology and Earth System Sciences*, 24, 1831–1858, <https://doi.org/10.5194/hess-24-1831-2020>, 2020.
- Berkowitz, B., Cortis, A., Dentz, M., and Scher, H.: Modeling non-Fickian transport in geological formations as a continuous time random walk, *Reviews of Geophysics*, 44, 2006.
- 780 Beven, K.: A manifesto for the equifinality thesis, *Journal of Hydrology*, 320, 18–36, <https://doi.org/10.1016/j.jhydrol.2005.07.007>, 2006.
- Beven, K. and Germann, P.: Macropores and water flow in soils, *Water resources research*, 18, 1311–1325, 1982.
- Bianchi, M., Zheng, C., Wilson, C., Tick, G. R., Liu, G., and Gorelick, S. M.: Spatial connectivity in a highly heterogeneous aquifer: From cores to preferential flow paths, *Water Resources Research*, 47, 2011.
- Birkel, C., Soulsby, C., and Tetzlaff, D.: Modelling catchment-scale water storage dynamics: Reconciling dynamic storage with tracer inferred 785 passive storage, *Hydrological Processes*, 25, 3924–3936, <https://doi.org/10.1002/hyp.8201>, 2011a.
- Birkel, C., Tetzlaff, D., Dunn, S. M., and Soulsby, C.: Using lumped conceptual rainfall–runoff models to simulate daily isotope variability with fractionation in a nested mesoscale catchment, *Advances in Water Resources*, 34, 383–394, 2011b.
- Birkel, C., Soulsby, C., and Tetzlaff, D.: Conceptual modelling to assess how the interplay of hydrological connectivity, catchment storage and tracer dynamics controls nonstationary water age estimates, *Hydrological Processes*, 29, 2956–2969, 2015.
- 790 Blöschl, G., Blaschke, A. P., Broer, M., Bucher, C., Carr, G., Chen, X., Eder, A., Exner-Kittridge, M., Farnleitner, A., Flores-Orozco, A., Haas, P., Hogan, P., Kazemi Amiri, A., Oismüller, M., Parajka, J., Silasari, R., Stadler, P., Strauss, P., Vreugdenhil, M., and Zessner, M.: The Hydrological Open Air Laboratory (HOAL) in Petzenkirchen: a hypothesis-driven observatory, *Hydrology and Earth System Sciences*, 20, 227–255, <https://doi.org/10.5194/hess-20-227-2016>, 2016.

- 795 Bogena, H. R., Bol, R., Borchard, N., Brüggemann, N., Diekkrüger, B., Drüe, C., Groh, J., Gottselig, N., Huisman, J. A., Lücke, A., et al.: A  
terrestrial observatory approach to the integrated investigation of the effects of deforestation on water, energy, and matter fluxes, *Science  
China Earth Sciences*, 58, 61–75, 2015.
- Bogena, H. R., Montzka, C., Huisman, J. A., Graf, A., Schmidt, M., Stockinger, M., von Hebel, C., Hendricks-Franssen, H. J., van der Kruk,  
J., Tappe, W., Lücke, A., Baatz, R., Bol, R., Groh, J., Pütz, T., Jakobi, J., Kunkel, R., Sorg, J., and Vereecken, H.: The TERENORur  
Hydrological Observatory: A Multiscale MultiCompartment Research Platform for the Advancement of Hydrological Science, *Vadose  
800 Zone Journal*, 17, 1–22, <https://doi.org/10.2136/vzj2018.03.0055>, 2018.
- Bogena, H. R., Stockinger, M. P., and Lücke, A.: Long-term stable water isotope and runoff data for the investigation of deforestation effects  
on the hydrological system of the Wüstebach catchment, Germany, *Hydrological processes*, 35, e14 006, 2021.
- Borriero, A., Kumar, R., Nguyen, T. V., Fleckenstein, J. H., and Lutz, S. R.: Uncertainty in water transit time estimation with StorAge  
Selection functions and tracer data interpolation, *Hydrology and Earth System Sciences*, 27, 2989–3004, [https://doi.org/10.5194/hess-27-  
2989-2023](https://doi.org/10.5194/hess-27-<br/>805 2989-2023), 2023.
- Botter, G., Bertuzzo, E., and Rinaldo, A.: Catchment residence and travel time distributions: The master equation, *Geophysical Research  
Letters*, 38, 1–6, <https://doi.org/10.1029/2011GL047666>, 2011.
- Exner-Kittridge, M., Strauss, P., Blöschl, G., Eder, A., Saracevic, E., and Zessner, M.: The seasonal dynamics of the stream sources and  
input flow paths of water and nitrogen of an Austrian headwater agricultural catchment, *Science of the Total Environment*, 542, 935–945,  
810 <https://doi.org/10.1016/j.scitotenv.2015.10.151>, 2016.
- Fenicia, F., Savenije, H. H., Matgen, P., and Pfister, L.: Is the groundwater reservoir linear? Learning from data in hydrological modelling,  
*Hydrology and Earth System Sciences*, 10, 139–150, <https://doi.org/10.5194/hess-10-139-2006>, 2006.
- Fenicia, F., Wrede, S., Kavetski, D., Pfister, L., Hoffmann, L., Savenije, H. H., and McDonnell, J. J.: Assessing the impact of mixing  
assumptions on the estimation of streamwater mean residence time, *Hydrological Processes*, 24, 1730–1741, 2010.
- 815 Florianic, M. G., Stockinger, M. P., Kirchner, J. W., and Stumpp, C.: Monthly new water fractions and their relationships with climate and  
catchment properties across Alpine rivers, *Hydrology and Earth System Sciences*, 28, 3675–3694, 2024.
- Fovet, O., Ruiz, L., Hrachowitz, M., Faucheux, M., and Gascuel-Odoux, C.: Hydrological hysteresis and its value for assessing process  
consistency in catchment conceptual models, *Hydrology and Earth System Sciences*, 19, 105–123, 2015.
- Graf, A., Bogena, H. R., Drüe, C., Hardelauf, H., Pütz, T., Heinemann, G., and Vereecken, H.: Spatiotemporal relations between  
820 water budget components and soil water content in a forested tributary catchment, *Water Resources Research*, 50, 4837–4857,  
<https://doi.org/10.1002/2013wr014516>, 2014.
- Hamilton, S. K.: Biogeochemical time lags may delay responses of streams to ecological restoration, *Freshwater Biology*, 57, 43–57, 2012.
- Hansen, S. K. and Berkowitz, B.: Aurora: A non-Fickian (and Fickian) particle tracking package for modeling groundwater contaminant  
transport with MODFLOW, *Environmental Modelling & Software*, 134, 104 871, 2020a.
- 825 Hansen, S. K. and Berkowitz, B.: Modeling non-Fickian solute transport due to mass transfer and physical heterogeneity on arbitrary ground-  
water velocity fields, *Water Resources Research*, 56, e2019WR026 868, 2020b.
- Harman, C.: Age-ranked storage-discharge relations: A unified description of spatially lumped flow and water age in hydrologic systems,  
*Water Resources Research*, 55, 7143–7165, 2019.
- Harman, C. J.: Time-variable transit time distributions and transport: Theory and application to storage-dependent transport of chloride in a  
830 watershed, *Water Resources Research*, 51, 1–30, 2015.

- Hövel, A., Stumpp, C., Bogena, H., Lücke, A., Strauss, P., Blöschl, G., and Stockinger, M.: Repeating patterns in runoff time series: A basis for exploring hydrologic similarity of precipitation and catchment wetness conditions, *Journal of Hydrology*, 629, 130–158, 2024.
- Hrachowitz, M., Savenije, H., Bogaard, T. A., Tetzlaff, D., and Soulsby, C.: What can flux tracking teach us about water age distribution patterns and their temporal dynamics?, *Hydrology and Earth System Sciences*, 17, 533–564, <https://doi.org/10.5194/hess-17-533-2013>, 2013.
- 835 Hrachowitz, M., Fovet, O., Ruiz, L., Euser, T., Gharari, S., Nijzink, R., Freer, J., Savenije, H., and Gascuel-Oudou, C.: Process consistency in models: The importance of system signatures, expert knowledge, and process complexity, *Water resources research*, 50, 7445–7469, 2014.
- Hrachowitz, M., Fovet, O., Ruiz, L., and Savenije, H. H.: Transit time distributions, legacy contamination and variability in biogeochemical  $1/f\alpha$  scaling: How are hydrological response dynamics linked to water quality at the catchment scale?, *Hydrological Processes*, 29, 5241–5256, <https://doi.org/10.1002/hyp.10546>, 2015.
- 840 Hrachowitz, M., Benettin, P., Breukelen, B. M. V., Fovet, O., Howden, N. J. K., Ruiz, L., Velde, Y. V. D., and Wade, A. J.: Transit times—The link between hydrology and water quality at the catchment scale, *Wiley Interdisciplinary Reviews: Water*, 3, 629–657, 2016.
- Hrachowitz, M., Stockinger, M., Coenders-Gerrits, M., Ent, R., Bogena, H., Lücke, A., and Stumpp, C.: Reduction of vegetation-accessible 845 water storage capacity after deforestation affects catchment travel time distributions and increases young water fractions in a headwater catchment, *Hydrology and Earth System Sciences*, 25, 4887–4915, <https://doi.org/10.5194/hess-25-4887-2021>, 2021.
- Janos, D., Molson, J., and Lefebvre, R.: Regional groundwater flow dynamics and residence times in Chaudière-Appalaches, Québec, Canada: insights from numerical simulations, *Canadian Water Resources Journal/Revue canadienne des ressources hydriques*, 43, 214–239, 2018.
- Jothityangkoon, C., Sivapalan, M., and Farmer, D.: Process controls of water balance variability in a large semi-arid catchment: downward 850 approach to hydrological model development, *Journal of hydrology*, 254, 174–198, 2001.
- Kaandorp, V. P., de Louw, P. G. B., van der Velde, Y., and Broers, H. P.: Transient Groundwater Travel Time Distributions and Age-Ranked Storage-Discharge Relationships of Three Lowland Catchments, *Water Resources Research*, 54, 4519–4536, <https://doi.org/10.1029/2017wr022461>, 2018a.
- Kaandorp, V. P., Molina-Navarro, E., Andersen, H. E., Bloomfield, J. P., Kuijper, M. J., and de Louw, P. G.: A conceptual model for the 855 analysis of multi-stressors in linked groundwater–surface water systems, *Science of the Total Environment*, 627, 880–895, 2018b.
- Kirchner, J. W.: Aggregation in environmental systems-Part 1: Seasonal tracer cycles quantify young water fractions, but not mean transit times, in spatially heterogeneous catchments, *Hydrology and Earth System Sciences*, 20, 279–297, <https://doi.org/10.5194/hess-20-279-2016>, 2016.
- Kirchner, J. W., Benettin, P., and van Meerveld, I. V.: Instructive Surprises in the Hydrological Functioning of Landscapes, 860 <https://doi.org/10.1146/annurev-earth-071822>, 2023.
- Klaus, J. and McDonnell, J. J.: Hydrograph separation using stable isotopes: Review and evaluation, *Journal of Hydrology*, 505, 47–64, 2013.
- Klaus, J., Zehe, E., Elsner, M., Külls, C., and McDonnell, J.: Macropore flow of old water revisited: experimental insights from a tile-drained hillslope, *Hydrology and Earth System Sciences*, 17, 103–118, 2013.
- 865 Knighton, J., Souter-Kline, V., Volkmann, T., Troch, P. A., Kim, M., Harman, C. J., Morris, C., Buchanan, B., and Walter, M. T.: Seasonal and topographic variations in ecohydrological separation within a small, temperate, snow-influenced catchment, *Water Resources Research*, 55, 6417–6435, 2019.
- Kuppel, S., Tetzlaff, D., Maneta, M. P., and Soulsby, C.: ECH2O-iso 1.0: Water isotopes and age tracking in a process-based, distributed ecohydrological model, *Geoscientific Model Development*, 11, 3045–3069, <https://doi.org/10.5194/gmd-11-3045-2018>, 2018.

- Loritz, R., Hassler, S. K., Jackisch, C., Allroggen, N., Van Schaik, L., Wienhöfer, J., and Zehe, E.: Picturing and modeling catchments by representative hillslopes, *Hydrology and Earth System Sciences*, 21, 1225–1249, 2017.
- Maxwell, R. M., Condon, L. E., Kollet, S. J., Maher, K., Haggerty, R., and Forrester, M. M.: The imprint of climate and geology on the residence times of groundwater, *Geophysical Research Letters*, 43, 701–708, 2016.
- Maxwell, R. M., Condon, L. E., Danesh-Yazdi, M., and Bearup, L. A.: Exploring source water mixing and transient residence time distributions of outflow and evapotranspiration with an integrated hydrologic model and Lagrangian particle tracking approach, *Ecohydrology*, 12, e2042, <https://doi.org/10.1002/eco.2042>, 2019.
- McGuire, K. J. and McDonnell, J. J.: A review and evaluation of catchment transit time modeling, *Journal of Hydrology*, 330, 543–563, 2006.
- McMillan, H., Tetzlaff, D., Clark, M., and Soulsby, C.: Do time-variable tracers aid the evaluation of hydrological model structure? A multimodel approach, *Water Resources Research*, 48, 2012.
- Nash, J. E. and Sutcliffe, J. V.: River flow forecasting through conceptual models part I—A discussion of principles, *Journal of hydrology*, 10, 282–290, 1970.
- Pavlin, L., Széles, B., Strauss, P., Blaschke, A. P., and Blöschl, G.: Event and seasonal hydrologic connectivity patterns in an agricultural headwater catchment, *Hydrology and Earth System Sciences*, 25, 2327–2352, <https://doi.org/10.5194/hess-25-2327-2021>, 2021.
- Rinaldo, A., Benettin, P., Harman, C. J., Hrachowitz, M., McGuire, K. J., van der Velde, Y., Bertuzzo, E., and Botter, G.: Storage selection functions: A coherent framework for quantifying how catchments store and release water and solutes, *Water Resources Research*, 51, 4840–4847, 2015.
- Salmon-Monviola, J., Fovet, O., and Hrachowitz, M.: Improving the hydrological consistency of a process-based solute-transport model by simultaneous calibration of streamflow and stream concentrations, *Hydrology and Earth System Sciences*, 29, 127–158, 2025.
- Sprenger, M., Leistert, H., Gimbel, K., and Weiler, M.: Illuminating hydrological processes at the soil-vegetation-atmosphere interface with water stable isotopes, *Reviews of Geophysics*, 54, 674–704, 2016.
- Stewart, M. K. and Morgenstern, U.: Importance of tritium-based transit times in hydrological systems, *Wiley Interdisciplinary Reviews: Water*, 3, 145–154, 2016.
- Stockinger, M. P., Bogen, H. R., Lücke, A., Diekkrüger, B., Weiler, M., and Vereecken, H.: Seasonal soil moisture patterns: Controlling transit time distributions in a forested headwater catchment, *Water Resources Research*, 50, 5270–5289, 2014.
- Stockinger, M. P., Bogen, H. R., Lücke, A., Diekkrüger, B., Cornelissen, T., and Vereecken, H.: Tracer sampling frequency influences estimates of young water fraction and streamwater transit time distribution, *Journal of hydrology*, 541, 952–964, 2016.
- Stockinger, M. P., Bogen, H. R., Lücke, A., Stumpp, C., and Vereecken, H.: Time variability and uncertainty in the fraction of young water in a small headwater catchment, *Hydrology and Earth System Sciences*, 23, 4333–4347, <https://doi.org/10.5194/hess-23-4333-2019>, 2019.
- Storn, R. and Price, K.: Differential evolution—a simple and efficient heuristic for global optimization over continuous spaces, *Journal of global optimization*, 11, 341–359, 1997.
- Széles, B., Parajka, J., Hogan, P., Silasari, R., Pavlin, L., Strauss, P., and Blöschl, G.: The Added Value of Different Data Types for Calibrating and Testing a Hydrologic Model in a Small Catchment, *Water Resources Research*, 56, <https://doi.org/10.1029/2019WR026153>, 2020.
- Türk, H., Stumpp, C., Hrachowitz, M., Schulz, K., Strauss, P., Blöschl, G., and Stockinger, M.: Soil moisture and precipitation intensity control the transit time distribution of quick flow in a flashy headwater catchment, *Hydrology and Earth System Sciences Discussions*, 2024, 1–33, 2024.

- van der Velde, Y., Rozemeijer, J. C., De Rooij, G. H., van Geer, F. C., Torfs, P. J. J. F., and de Louw, P. G. B.: Improving catchment discharge predictions by inferring flow route contributions from a nested-scale monitoring and model setup, *Hydrology and Earth System Sciences*, 15, 913–930, <https://doi.org/10.5194/hess-15-913-2011>, 2011.
- 910 van der Velde, Y., Torfs, P. J. J. F., van der Zee, S. E. A. T. M., and Uijlenhoet, R.: Quantifying catchment-scale mixing and its effect on time-varying travel time distributions, *Water Resources Research*, 48, <https://doi.org/10.1029/2011WR011310>, 2012.
- van der Velde, Y., Heidbüchel, I., Lyon, S., Nyberg, L., Rodhe, A., Bishop, K., and Troch, P.: Consequences of mixing assumptions for time-variable travel time distributions, *Hydrological Processes*, 29, 3460–3474, <https://doi.org/10.1002/hyp.10372>, 2015.
- Visser, A., Heerdink, R., Broers, H., and Bierkens, M.: Travel time distributions derived from particle tracking in models containing weak sinks, *Groundwater*, 47, 237–245, 2009.
- 915 Vreugdenhil, M., Széles, B., Wagner, W., Strauß, P., Oismueller, M., Parajka, J., Blöschl, G., and Hogan, P.: Non-linearity in event runoff generation in a small agricultural catchment, *Hydrological Processes*, pp. 1–16, <https://doi.org/10.1002/hyp.14667>, 2022.
- Wang, S., Hrachowitz, M., Schoups, G., and Stumpp, C.: Stable water isotopes and tritium tracers tell the same tale: no evidence for underestimation of catchment transit times inferred by stable isotopes in StorAge Selection (SAS)-function models, *Hydrology and Earth System Sciences*, 27, 3083–3114, 2023.
- 920 Wang, S., Hrachowitz, M., Schoups, G., and Störiko, A.: Multi-decadal stability of water ages and tracer transport in a temperate-humid river basin, *Environmental Research Letters*, 2025.
- Weiler, M., McGlynn, B. L., McGuire, K. J., and McDonnell, J. J.: How does rainfall become runoff? A combined tracer and runoff transfer function approach, *Water Resources Research*, 39, <https://doi.org/10.1029/2003WR002331>, 2003.
- Wiekenkamp, I., Huisman, J. A., Bogena, H. R., Graf, A., Lin, H. S., Drüe, C., and Vereecken, H.: Changes in measured spatiotemporal 925 patterns of hydrological response after partial deforestation in a headwater catchment, *Journal of Hydrology*, 542, 648–661, 2016.
- Yadav, M., Wagener, T., and Gupta, H.: Regionalization of constraints on expected watershed response behavior for improved predictions in ungauged basins, *Advances in water resources*, 30, 1756–1774, 2007.
- Zehe, E., Lee, H., and Sivapalan, M.: Dynamical process upscaling for deriving catchment scale state variables and constitutive relations for meso-scale process models, *Hydrology and Earth System Sciences*, 10, 981–996, 2006.
- 930 Zehe, E., Loritz, R., Edery, Y., and Berkowitz, B.: Preferential pathways for fluid and solutes in heterogeneous groundwater systems: self-organization, entropy, work, *Hydrology and earth system sciences*, 25, 5337–5353, 2021.
- Zuber, A.: On the interpretation of tracer data in variable flow systems, *Journal of Hydrology*, 86, 45–57, 1986.